MECHANICAL MODELLING AND DESIGN OF THE 4 FINGERS OF AN ANTHROPOMORPHIC ROBOTIC HAND

by

Muhammad Munzer Alseed

B.S., in Biomedical Engineering, Near East University, 2017

Submitted to the Institute of Biomedical Engineering
in partial fulfillment of the requirements
for the degree of
Master of Science
in
Biomedical Engineering

Boğaziçi University
2020

ACKNOWLEDGMENTS

First of all, I would like to express my sincere gratitude to my advisor, Prof. Dr. Mehmed Özkan, for all his encouragement, great support, and wise guidance for my M.S. thesis, for his patience, motivation, and immense help throughout my study at Boğaziçi University. I would not be able to make it so far without his generosity.

I also would like to thank Assoc. Prof. Dr. Erkan Kaplanoğlu for his unlimited support and encouragement throughout my academic journey.

Additionally, I would like to thank my labmates, Ahmet Atasoy, Gülfize Coskun, Shavkat Kuchimov, and Hasan Şahin, for their continuous assistance and great information that helped me conduct this study and write my thesis.

My heartfelt thanks go to my wonderful family as well as my loving wife, Loubaba Damen, for all kinds of support they have offered me, and for their encouragement, trust, and endless love.

ACADEMIC ETHICS AND INTEGRITY STATEMENT

I, Muhammad Munzer Alseed, hereby certify that I am aware of the Academic Ethics and Integrity Policy issued by the Council of Higher Education (YÖK) and I fully acknowledge all the consequences due to its violation by plagiarism or any other way.

Name :

Signature:

Date:

ABSTRACT

MECHANICAL MODELLING AND DESIGN OF THE 4 FINGERS OF AN ANTHROPOMORPHIC ROBOTIC HAND

Anthropomorphic robotic hands aim to resemble the functions and appearance of human hands. The increasing interest in their design arises from their importance in many medical and engineering applications. Controlling flexion and extension of each of the 4 fingers of an anthropomorphic robotic hand requires 3 motors to have full control of its joints. This study aims to construct a model for the 4 fingers to enable full control of all of their joints using only 2 motors by utilizing the correlation between proximal interphalangeal (PIP) and distal interphalangeal (DIP) joints of human finger to use a single motor for their control. A mechanical model is established for a single finger with correlated PIP and DIP joints to be generalized for the 4 fingers. Inverse kinematics is solved for the angles of the joints in terms of fingertip position. Transfer functions are derived for the change in tendons lengths during flexion to find the appropriate design of the pulleys controlling them. Hand parts are designed, 3D printed, and assembled accordingly, and then controlled using an Arduino microcontroller. Joints angles of the 4 fingers are measured over their full range of motion to calculate their correlation. Inverse kinematics gives a unique solution for each different fingertip position, but the ratio between the correlated angles should be assumed slightly different than that of a human hand for an algebraic solution to exist. The derived transfer functions are found to be nonlinear and increasing, meaning that the designed pulleys need to be spiral instead of perfectly circular. However, circular pulleys are used for the designed hand for simplification. Measured PIP and DIP joint angles show strong correlations for all fingers and over the full range of motion for all joints.

Keywords: Robotics, Anthropomorphic Hands, Interphalangeal Joints Correlation, Inverse Kinematics.

ÖZET

ANTROPOMORFİK ROBOT ELİN 4 PARMAK MEKANİK MODELLENMESİ VE TASARIMI

Antropomorfik (insansı) robotik el çalışmaları, amputeler için robot elin insan eline benzetilmesini ve elin işlevlerini yerine getirilmesini amaçlamaktadır. İnsansı elin her bir parmağın fleksiyon ve ekstansiyon hareketleri için 3 eklem için 3 motor ile kontrol edilmesi gerekir. Bu çalışmada tam kontrol için insan 4 parmağının Proksimal interfalangeal eklem (PIP) ve Distal İnterfalangeal eklem (DIP) eklemleri arasındaki ilişkiden yararlanılarak her bir parmak için 3 yerine 2 motor kullanılarak mekanik bir model oluşturulmuştur. Kuvvet , servo motor ve kasnaklar ile kontrol edilerek tendonlarla parmak eklemlerine iletilir. Her bir parmak pozisyonu için ters kinematik hesaplanmış fleksiyon ve ekstansiyon hareketlerinin farkı açılarda tendon uzunlukları için transfer fonksiyonu çıkartılarak kasnakların uygun geometrik tasarımı oluşturulmuştur. İnsansı elin parçaları bu modele uygun olarak tasarlanmış, üç boyutlu yazıcı ile basılıp birleştirilmiştir. Kontrolü Arduino mikrodenetleyicisi ile yapılmıştır. 4 parmağın eklem açıları, hareket açıklıkları boyunca ölçümüş ve eklemler arası ilişki hesaplanmıştır. Ters kinematik analiz her farklı parmak ucu pozisyonu için benzersiz bir çözüm sunar, ancak cebrisel bir çözüme ulaşmak için PIP ve DIP arasındaki ilişkiye ait oran insan elinden biraz farklı olduğu varsayılmıştır. Türetilmiş transfer fonksiyonu doğrusal olmayan ve artan bir ilişkiyi ortaya çıkarmıştır. Bu da tam dairesel kasnak yerine spiral olması gerektiğini gösterir. Bununla birlikte tasarımı basitleştirmek için dairesel kasnaklar kulanılmıştır. Ölçülen PIP ve DIP eklem açıları tüm parmakların hareket açıkıkları boyunca kuvvetli bir ilişkiyi göstermiştir.

Anahtar Sözcükler: Robotik, İnsansı el, İnterflakans eklem korelasyonu, ters kinematik.

TABLE OF CONTENTS

LIST OF FIGURES

LIST OF TABLES

LIST OF ABBREVIATIONS

2D	Two-Dimensional
3D	Three-Dimensional
ABS	Acrylonitrile Butadiene Styrene
BLDC	Direct Current Brushless
CMC	Carpometacarpal
CT	Computed Tomography
DC	Direct Current
DIP	Distal Interphalangeal
DOF	Degree of Freedom
IDE	Integrated Development Environment
IP	Interphalangeal
MCP	Metacarpophalangeal
MRI	Magnetic Resonance Imaging
PIP	Proximal Interphalangeal
PLA	Polylactic Acid
PWM	Pulse-Width Modulation
USB	Universal Serial Bus

1. INTRODUCTION

1.1 Motivation

Biomechatronics is a trending field of both industry and research, since it is achieving great improvements in rehabilitation, mainly in replacing amputees' limbs. The robotic hands available in the market have the ability to perform various tasks with high reliability and accuracy, and have quite robust designs. However, a large number of them are not anthropomorphic; i.e. they do not try to mimic the natural human hand in both anatomy and functionality, but they are almost totally dependent on the design itself from a mechanical point of view. Nevertheless, a remarkable effort has been made in the research literature to enhance the design and control of anthropomorphic hands. The results of such efforts are pronounced in fairly advanced robotic hands with complex designs and functions that are similar to those of a human hand.

However, one problem arises when the motion of PIP and DIP joints of the four fingers is considered. That is, there is a tradeoff between the instantaneous angles of those joints and cost in terms of power consumption, weight and price. If one tendon is attached to the distal phalanx and controlled by one motor is used to flex a single finger, the angles of PIP and DIP joints would be arbitrary during flexion, and a full control of both joints could not be achieved since 2 degrees of freedom are present but only one actuator is used. The only guaranteed fact is that the joints will be fully extended at their maximum extension position and vice versa for their flexion. To overcome this problem, two separate motors can control their corresponding tendons which are independently attached to the distal and middle phalanges, and this can produce precise control of PIP and DIP joints during finger flexion and extension. The drawback of the latter approach is using a second motor, which lays a doubled cost especially when it is applied on the four fingers.

1.2 Objectives

The main purpose of this thesis is to introduce an efficient way to fully control both PIP and DIP joints of the four fingers of an anthropomorphic hand. The aim is to avoid the randomness of the angles of those joints during flexion, as well as to reduce the cost of using extra motor. For this purpose, a correlation between human PIP and DIP angles that was found in the literature is utilized to design an anthropomorphic robotic hand [6]. This correlation is first modelled and simulated, and then implemented physically on a designed hand.

1.3 Thesis Outline

This thesis is divided into 5 chapters. In Chapter 2, background information about the hand anatomy and physiology is introduced. This includes explanation of the basic structures found in a human hand and their functionality of performing different tasks. In addition, the concept of anthropomorphic hands is introduced with some examples of existing hands and the different approaches used in their design. The related research papers utilized in this thesis to optimize the design are also given. Chapter 3 explains the methodology of modelling, designing, and implementing the hand, as well as the materials and tools used for this purpose. The final results of modelling and implementation are given in Chapter 4. Finally, the results are discussed in Chapter 5, along with the advantages and limitations of the design, with suggested improvements and future work that can be done.

2. BACKGROUND

In this chapter, brief information about the anatomy and functions of human hand is given. Additionally, anthropomorphic robotic hands are discussed, and the research papers on which this thesis relies are also introduced.

2.1 Human Hand

The human hand is a very complex organ that serves in performing different motor and sensory tasks. Both left and right hands are extremely essential in helping the human manipulate objects, change their shapes or positions, collect resources in the environment, and use tools to gather such resources and provide protection. These functions and many others are achieved by the ability of the human hand to grasp objects in the reach of the arm benefiting from its 27 degrees of freedom [7]. This can also provide alternative input or output assistance for impaired people, such as helping visually impaired people read braille texts, and enabling people with hearing or speech loss communicate with others using sign language. Sensory feedback of the hand is significantly helpful in identifying objects and extracting physical information about their shape, weight, texture, weight, size, orientation, compliance and temperature [8].

A healthy human hand has five digits, the first being the thumb, followed by the index finger, the middle finger, the ring finger and the little finger. The thumb has 5 degrees of freedom giving humans a great functional advantage. Each one of the other 4 fingers has 4 degrees of freedom; 3 for flexion and extension and one for adduction and abduction. The other 6 DOFs of the hand are left for the translation and rotation of the wrist [8]. Figure 2.1 shows the bones of a human hand [1].

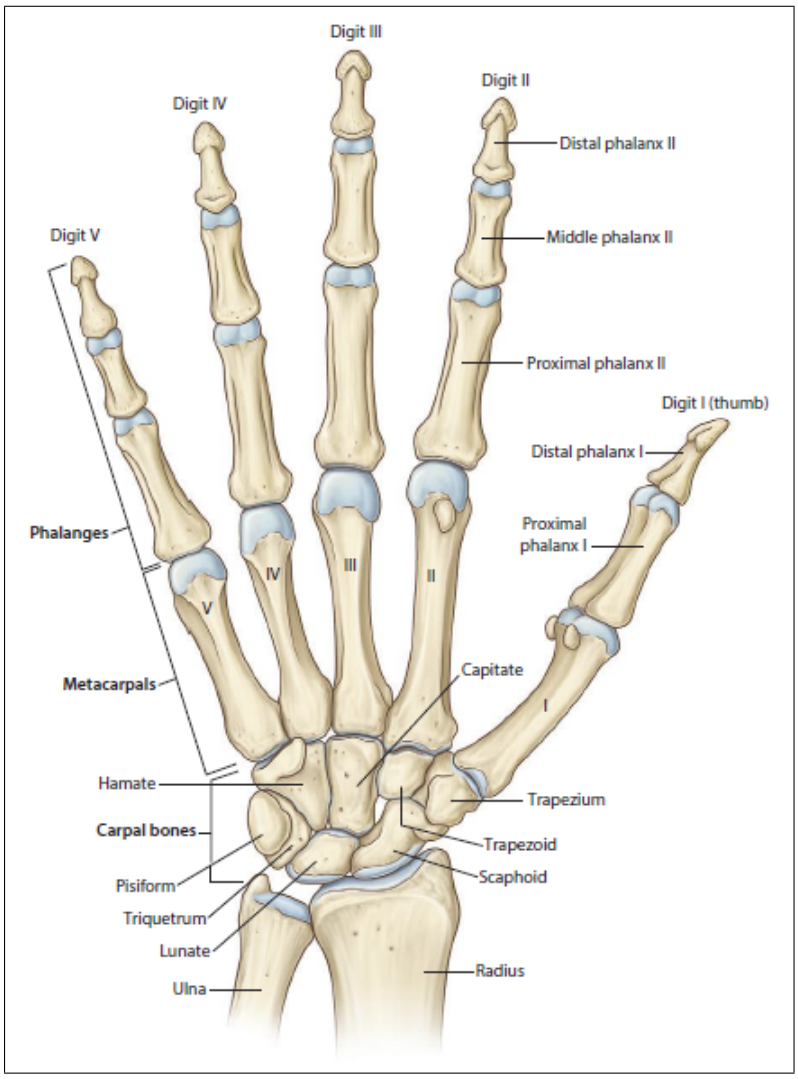

Figure 2.1 Bones of the human hand [1].

2.2 Human Finger

Fingers are the 4 digits other than the thumb. In spite of having different sizes and functions, they all share similar mechanical properties with their shared 4 DOFs. The thumb, on the other hand, serves different functions and has different anatomical and mechanical properties with its distal and proximal phalanges connected by the interphalangeal (IP) joint. The proximal phalanx is connected to the metacarpal bone by the metacarpophalangeal (MCP) joint, which enables the thumb to flex and extend along with the IP joint. The metacarpal bone can perform rotation on 3 axes by the carpometacarpal (CMC) joint [8],[9].

A typical human finger consists of three bones, which are the proximal, middle, and distal phalanges. These phalanges are connected through two interphalangeal joints, by which extension and flexion occurs, and these joints are the proximal interphalangeal (PIP) joint and the distal interphalangeal (DIP) joint. The force required for motion is transmitted from the forearm muscles to the phalanges by tendons, which can be flexors or extensors. Flexor tendons extend from the anterior forearm muscles and pass from the volar side of the hand and attach to their respective insertion points of the finger phalanges, while extensor tendons emerge from the posterior forearm muscles and attach to the phalanges passing from the dorsal side of the hand. Tendons are held in place by means of special ligaments known as retinacular ligaments, which provide an efficient tunneling system for the tendons to pass underneath them tightly [10]. The proximal phalanx of each finger is able to flex, extend, adduct and abduct by means of the metacarpophalangeal (MCP) joint that connects it to the metacarpal bone located inside the palm of the hand. The 4 metacarpal bones are based on 8 carpal bones that connect to the ulna and radius joint located in the forearm creating the wrist or the radiocarpal joint [9]. Figure 2.2 shows the basic structures found in a human finger [2].

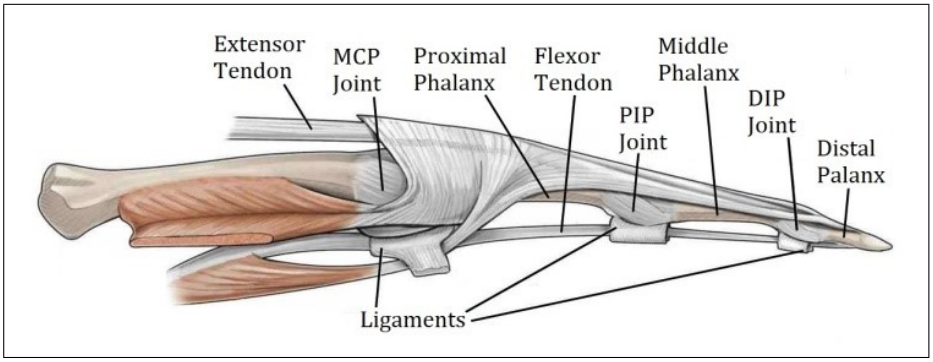

Figure 2.2 Bones, tendons and ligaments of a human finger [2].

2.3 Anthropomorphic Hands

Anthropomorphism is the ability of a non-human entity to resemble human traits, emotions, or intentions. Therefore, anthropomorphic robotic hands aim to mimic human hands in both anatomy and functionality. Although it is possible to design

robotic hands that can achieve far better dexterity than a human hand meaning less resemblance to it, anthropomorphic designs are more preferred for specific applications, as in prostheses that are intended to replace amputees' upper extremities, remotely controlled hands operated by a human, and humanoid robots. In spite of their physical limitations, the design of anthropomorphic hands can be optimized by studying the mechanical properties of human hands in vivo and applying that to robotics [11].

Many designs of anthropomorphic hands have been suggested and implemented in the literature and industry since the 1980s, following various approaches and having different levels of complexity. One of the recent anthropomorphic hands, which is considered to be the most advanced one so far, is the "Highly Biomimetic Anthropomorphic Robotic Hand". Its reputation comes from the realistic design of the hand phalanges that look exactly like the human ones, with detailed anatomical features like tendons, joints that utilize ligaments for a smooth motion, with an extensor hood and tendon sheaths that play a critical role in supporting the other parts and enhancing both anatomical appearance and functional abilities of the hand. This hand uses 10 servo motors to control the 5 fingers and can perform a wide variety of gestures allowing it to grasp objects of different sizes (Figure 2.3) [3].

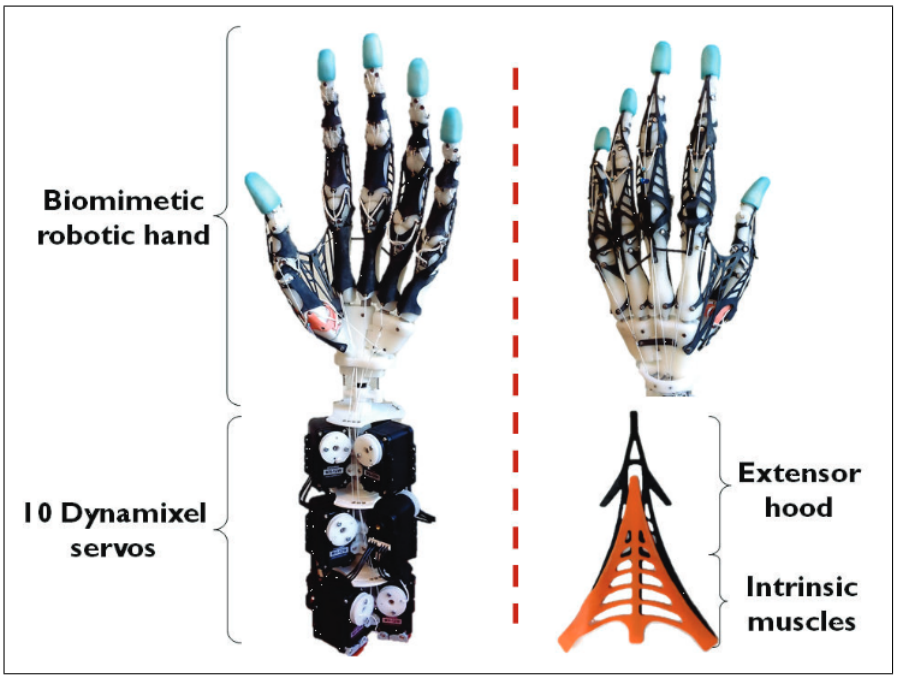

Figure 2.3 The Highly Biomimetic Anthropomorphic Robotic Hand [3].

Another recent anthropomorphic hand was developed at Boğaziçi University. The researchers used 13 BLDC motors that control the 5 digits and the wrist to provide high torque and controllability, and they came up with a design that gives more freedom for the metacarpal bones to slightly move as in the human hand. The usage of BLDC motors in the tendon-driven hand allows using the included hall sensors to provide real-time position information to be used for control purposes (Figure 2.4) [4].

Both of those hands use tendon-like strings to transmit the force from motors to fingers as mentioned above, as well as many other hands [12],[13],[14],[15]. Other force transmission methods involve using gears, belts, and other mechanical methods rather than tendons [16],[17],[18], which can be considered less anthropomorphic from an anatomical point of view. Different types of motors are used according to the applications, such as electrical motors [16],[19],[20] and pneumatic actuators [21],[22].

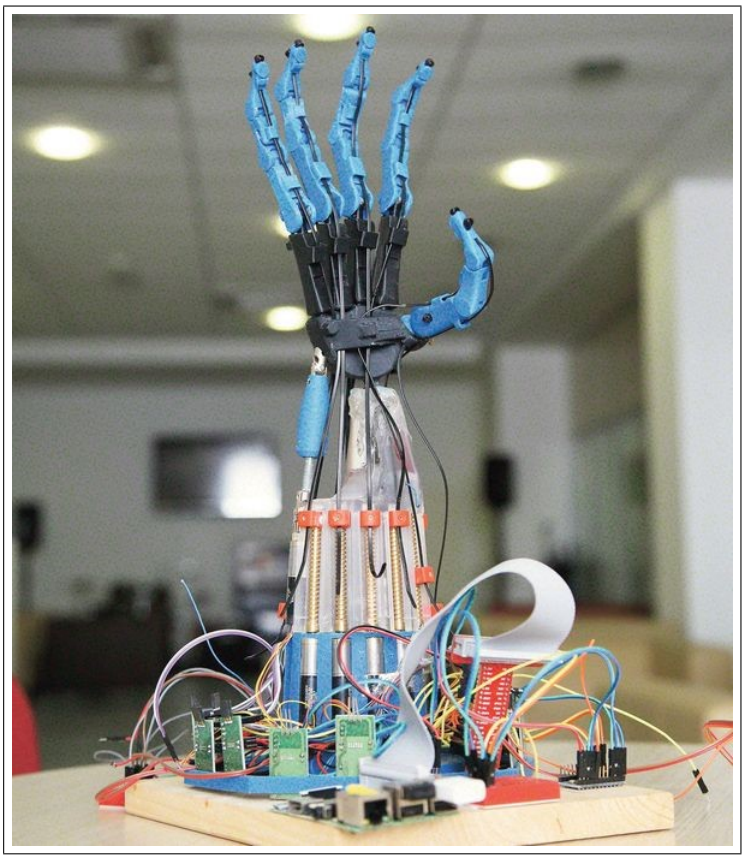

Figure 2.4 The anthropomorphic hand developed at Boğaziçi University [4].

2.4 Correlation between PIP and DIP Joint Angles

Many studies have shown that angles of PIP and DIP joints of each of the 4 fingers are strongly correlated during flexion and extension [6],[5],[23]. Van Zwieten et al. tried to find a mathematical expression that describes this correlation in healthy individuals, aiming to identify individuals showing pathologies. They used one healthy and one pathological datasets to establish a 2 dimensional kinematic model plotting PIP against DIP angles. Although their goal was not to calculate the correlation but to find an algebraic formula for the relationship, the non-linear plot of their fitted model (Figure 2.5) shows that DIP and PIP angles increase together [5].

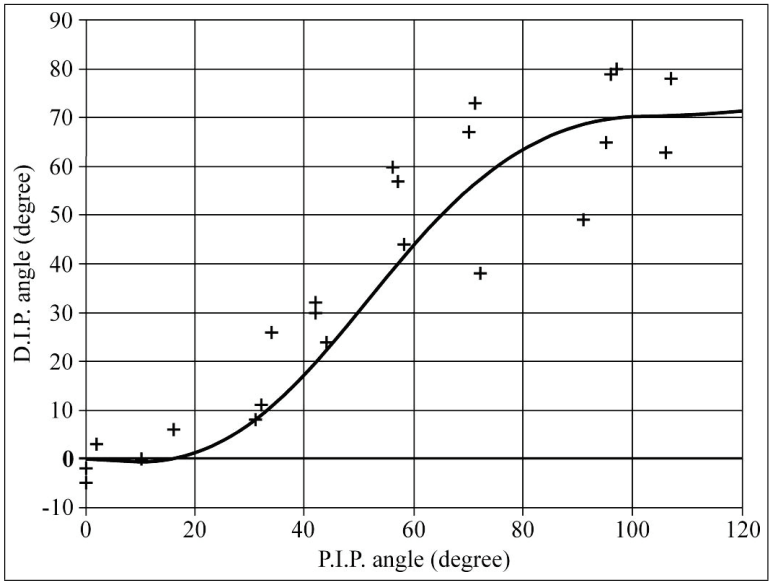

Figure 2.5 A fitted model of the relationship between of DIP and PIP angles [5].

A study conducted by Hahn et al. measured the angles of PIP and DIP joints during index finger flexion, and found a very high correlation of 0.986 between them. By looking at the plot provided by that study which shows data collected from several individuals (Figure 2.6) it can be noticed that the relationship between PIP and DIP joints is almost linear over the whole range of motion, except for the angles near the maximum and minimum of the range which vary among individuals with a small deviation [6].

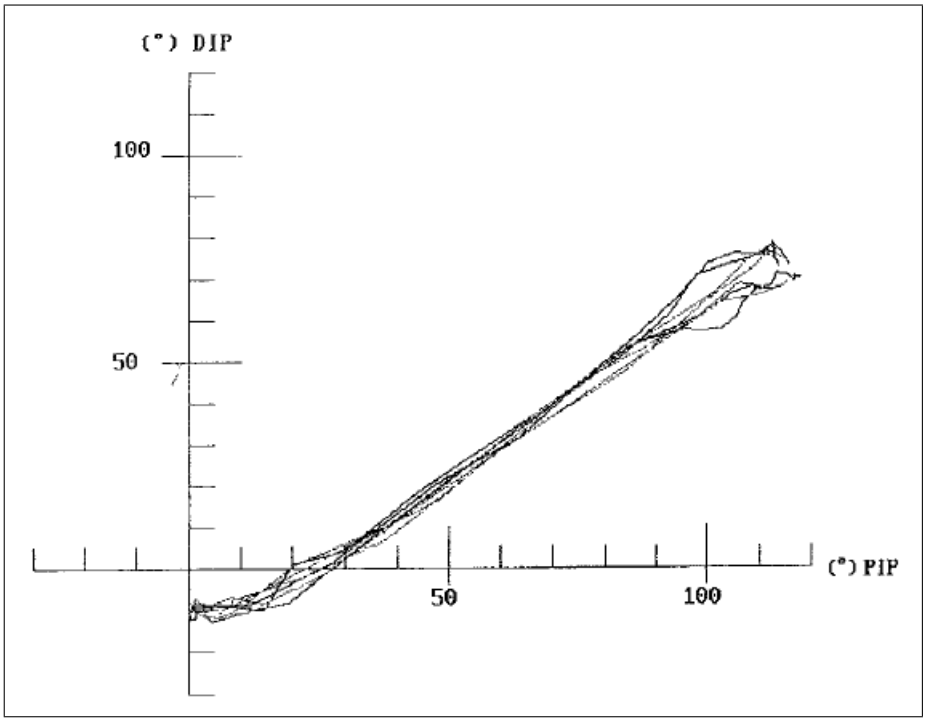

Figure 2.6 The correlation between PIP and DIP joints angles [6].

3. METHODS

The workflow of this thesis can be recognized as 6 main successive steps. First, a general model of a single finger is built to achieve the desired correlation between PIP and DIP joints and independence of MCP joint. Second, an inverse kinematic model is built to derive the required PIP, DIP and MCP angles that correspond to a specific fingertip position. Third, the relationship between the motors rotation and finger angles is derived through forward kinematics to relate motors rotation to fingertip position aiming to find the transfer functions. Next, the hand parts and pulleys used to convert the rotational motion of motors into a linear motion are designed and assembled based on the simplified kinematic model. After that, a microcontroller is used to control the 4 fingers and produce different gestures in order to test the ability of the hand to perform different types of motion and to show the correlation between PIP and DIP and the independence of MCP joint. Finally, the angles of PIP and DIP joints are measured during flexion to check if their desired correlation is achieved.

3.1 Modelling a Single Finger

A single mechanical model is built for all the fingers as they all share the same motions of flexion and extension, taking into account the differences in their lengths. Since only flexion and extension are considered, the constructed model is 2 dimensional.

For one finger, two non-elastic tendons are used; one to flex the PIP joint and another to extend the DIP joint. Extension of PIP and flexion of DIP are carried out using elastic tendons. One actuator is used to control both non-elastic tendons since their angles are correlated during motion. MCP joint is controlled by two non-elastic joints for its flexion and extension which transmit the force produced by a single actuator. Non-elastic tendons pass through tunnels added to the fingers to simulate retinacular ligaments. Elastic tendons are modelled to fulfill their passive functions by opposing the pulling of non-elastic tendons. Therefore, one elastic tendon connects

the distal and middle phalanges at their flexion side, while another one connects the middle and proximal phalanges at their extension side.

Figure 3.1 shows the established model of the finger. When motor 1 rotates to pull non-elastic tendon 2, its length decreases causing the flexion of PIP joint. At the same time, the length of non-elastic tendon 1 increases, allowing elastic tendon 1 to pull the distal and middle phalanges together and flex the DIP joint. Consequently, PIP and DIP joints can be flexed together using one motor, and they also extend together in a similar manner utilizing elastic tendon 2 and rotating the motor in the opposite direction.

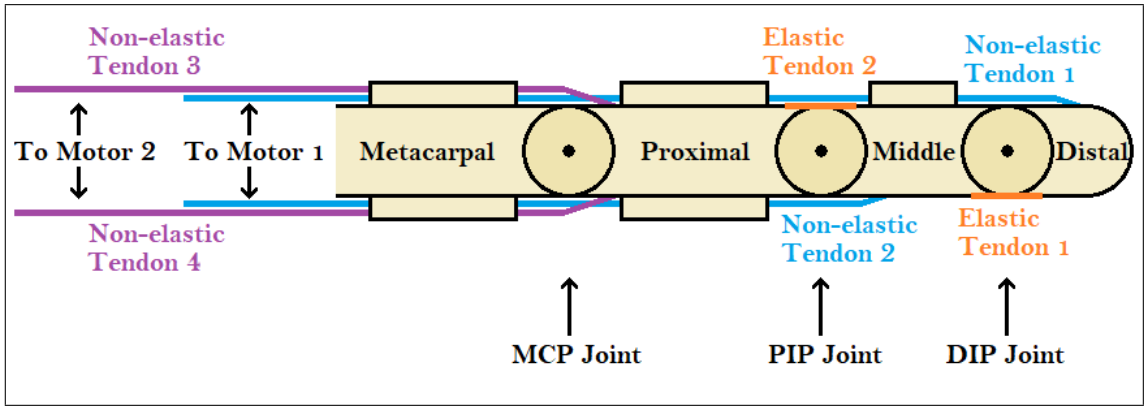

Figure 3.1 Mechanical Model of Finger.

3.2 Inverse Kinematics

A typical 3-joint planar robot arm model is used to solve the inverse kinematics of a single finger. However, the assumed linear correlation between PIP and DIP joints must be considered, which reduces the number of variable joint angles from 3 to 2, taking into account the range of motion of each joint to match those of human fingers [26]. After the algebraic formulas of the model are derived, they are implemented using Processing software to visualize the change in finger angles during flexion and extension. The simulation is built in such a way that makes the fingertip always following the mouse cursor on the screen, changing the finger angles accordingly.

3.3 Derivation of Transfer Functions

Results from the solution of the inverse kinematics are used in the derivation of transfer functions between motors rotation and finger angles. Some assumptions are made to simplify the model and to allow generalization over different fingers: Taking into account that the model is 2 dimensional, all phalanges are assumed to have the same width. The length of each phalanx therefore does not have any effect on the model, allowing it to be adopted for all fingers. Retinacular ligaments are taken to be symmetric around the joints, making an initial angle at full extension with the axis of rotation which is assumed to be the same for PIP and MCP joints. After deriving the transfer functions of the 4 non-elastic tendons, the relationship between them is plotted using MATLAB, and the solution of the inverse kinematics is added to produce the generalized transfer functions.

3.4 Hand Design and Assembly

Since the hand to be designed is intended to be anthropomorphic, the design of hand elements is considered to resemble those of a human being. The main elements the design is concerned with are bones, joints, retinacular ligaments, tendons, and pulleys, which need to be designed one after another, respectively.

3.4.1 Bones Design

To achieve the optimum anthropomorphism possible for the hand bones, they are chosen to have the same 3-dimensional shape of human bones. For this purpose, multiple options are available, such as utilizing data collected from MRI, CT or other types of scanning. However, MRI and CT scans taken in vivo would have some defects due to the interference with the surrounding tissues and structures, which requires further modification and gap filling, consuming more time and losing some information about the original shape. Better detailed 3D images of hand bones can be obtained by

taking the bones of a dead hand, cleaning them from any excess tissues and scanning them directly. This was actually done using a Next Engine Laser scanner and published publicly under the Creative Commons - Attribution - Share Alike license as 3D object files [24]. To use these files for the hand design, they are compared to hand bones photos found in anatomy books to ensure their validity [1],[9], and they are found to be valid for the whole design.

Printing the bone files is performed using a Zortrax 3D printer of the model M200. ULTRAT material is used for the prints, due to its relative flexibility compared to PLA which makes it less fragile; a quality of importance that arises when moving parts are involved such as joints in this case. It also shows less shrinkage rate than ABS material during printing, avoiding printing errors that eventually produce unusable prints [25]. The color of selection is ivory to give the bones a realistic look.

Bones that are connected with joints that have negligible motions are joined together to be printed as a single part. Although the thumb is outside the scope of this thesis, its bones are printed separately for demonstration. As a result, 16 distinct parts are printed to form a complete right hand: 5 distal phalanges, 4 middle phalanges, 5 proximal phalanges, 1 metacarpal of the thumb and one part that combines the remaining 4 metacarpals and the 8 carpal bones.

3.4.2 Joints Design

Joints of interest are designed to be able to perform flexion and extension. Other motions with which this thesis is not concerned are not considered, which are adduction and abduction, as they can create further complications and arbitrary motions. For each of the four fingers, three joints are added: DIP, PIP and MCP. The IP, MCP and CMC joints of the thumb are also added only for demonstration.

Since only flexion and extension are concerned, hinge joints are used. A single design is made and added for all joints using Microsoft 3D Builder software. The joint

is held in place by an axis of rotation made of a stainless-steel cylindrical pin with a diameter of 1 mm. Joint design and dimensions are shown in Figure 3.2.

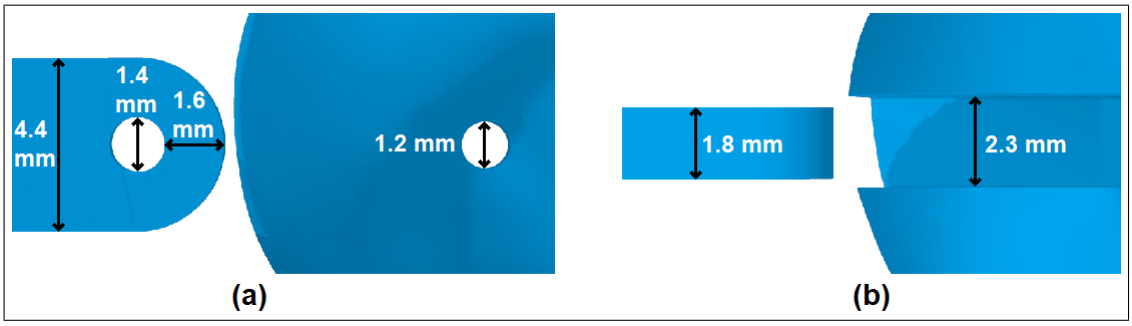

Figure 3.2 Joint design and dimensions. (a) Side view. (b) Upper view.

One important factor that should be considered while designing joints is range of motion. To include that in the hand design, joints are designed based on data collected from actual human hand by a study that measured normal and functional range of motion for each of the hand joints [26]. For this thesis, the normal range of motion is to be used for joint design, as it represents the maximum and minimum angles possible for each joint. Table 3.1 shows the normal range of motion of human hand joints. Note that the aforementioned study did not measure the range of motion of CMC joint, so it is designed to be 0-90°, as it is outside the scope of this thesis. Based on the results of that study, the joints are designed to have the same range of motion with additional 10 degrees for each joint to allow for slightly wider ranges.

Table 3.1
Normal range of motion of human hand [26].

Thumb		Fingers		
MCP	IP	MCP	PIP	DIP
0-56° (85% of the population) 0-27° (15% of the population)	5-73°	0-100°	0-105°	0-85°

After designing the joints and adding them to their corresponding bones properly, the bones are printed again to examine the functionality of each joint in terms of producing a smooth motion that is not interrupted by any obstacle, as well as being able to move over the whole range of motion without failing to reach the maximum

and minimum of that range. The distance between each two adjacent joints for every finger is then measured using the same software used for the design, rounded to the nearest integer and reported to be used for the Matlab model.

3.4.3 Retinacular Ligaments and Tendons Design

Two types of tendons are used: non-elastic and elastic. Industrial threads with a cross-sectional diameter of 1 mm are used as non-elastic tendons for their high bending compliance compared to other materials like plastic or metals, which is an important property that prevents tendons from acting as passive materials and adding extra forces to the system. Rubber bands are used as elastic tendons with a circular cross-section that has a diameter of 1 mm.

Tendons need to have freedom to change their lengths near joints to allow flexion and extension, while they must be held in place on the bone surface. This is done in humans using retinacular ligaments which act like tunnels that contain tendons inside. Here, those tunnels are designed using Solid Edge 3D modelling software. Each tunnel is shaped so that it follows the topology of each finger, with a fixed inner diameter over the length of each tunnel of 2 mm to reduce friction with tendons that have a cross-sectional diameter of 1 mm. Moreover, further friction can significantly affect the motion caused by tendons that pass adjacent to each other on the surfaces of metacarpal and proximal phalanges. This is avoided by dedicating one separate tunnel for each tendon. Friction between tendons can also occur in the wrist, so some small tunnels are also added. Starting and ending points of each tunnel are determined based on 2 criteria: joints should not stop their flexion before they reach their maximum possible flexion angles, and bones topology has to be considered. Therefore, after designing bones and joints, flexion and extension are simulated using Solid Edge and the dimensions of the tunnels are identified accordingly. For each finger, the middle phalanx has a single tunnel on the flexion side, and both metacarpal and proximal phalanges have 2 tunnels on the flexion side and another 2 on the extension side.

Elastic tendons should also have tunnels to pass through them. Such tunnels are created inside the phalanges instead of making them external, which does not affect their performance since they are meant to be passive elements. Each tunnel has a fixed diameter of 1.5 mm to contain an elastic tendon with a cross-sectional diameter of 1 mm. The PIP flexor attaches to the distal phalanx, passes through the middle phalanx and attaches to its proximal end. The DIP extender connects the distal end of the middle phalanx with the proximal end of the proximal phalanx passing through both of them. Figure 3.3 shows the tunneling system used in the design of the index finger.

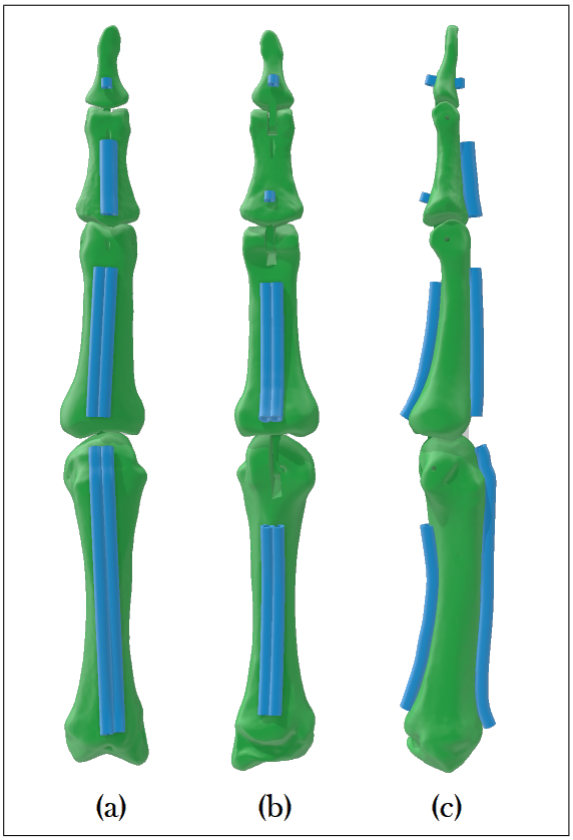

Figure 3.3 Tunneling system of the index finger. (a) Back view. (b) Front view. (c) Side view.

3.4.4 Pulleys Design

Converting the rotational motion of the motors to linear motion happens by means of pulleys. The usage of 2 motors corresponds to 2 pulleys. However, the resulted transfer functions show that tendons controlled by a single motor change

their lengths differently. This means that each motor should control 2 pulleys that rotate synchronously but have different perimeters. Transfer functions show non-linear relationships between PIP flexor and DIP extensor, as well as between MCP flexor and MCP extensor. This non-linearity involves trigonometric functions of multiple angles. Additionally, another dependency arises from the transfer functions between MCP angle and the rate of change of PIP and DIP angles. All of that makes modelling non-linear pulleys very complex especially with the geometric differences between the uniform modelled phalanges and the 3D printed phalanges that have uneven cross-sections for each one of them. For reasons of simplicity, pulleys are designed to produce linear transfer functions for every tendon pair, considering that the original non-linear functions are all monotonic and can be approximated to linear functions.

Each motor controls 2 circular pulleys designed as a single part, stacked over each other and given different diameters based on their lengths change during flexion and extension. The circular design is chosen to achieve linearity. Given the aforementioned differences between the mathematical model and the designed fingers, pulleys diameters are found by physical measurement of their lengths. All tendons are attached to their corresponding insertion points on the phalanges and passed through their dedicated tunnels. Every tendon is pulled and released to produce full flexion and full extension of the finger, and the change of its length is measured using a ruler accordingly. These changes are translated into pulley diameters, so that each pulley has a range of rotation equals to 2 radians or about 114.6 degrees.

The 3D models are designed using Microsoft 3D builder software. All pulleys have the same physical dimension except for their diameters which depend on their associated tendons. Every 2 pulleys controlled by the same motor are stacked over each other sharing the same center. To allow the motors to rotate the pulleys, a hole is designed in the middle of each double-pulley system so the motor shaft can fit tightly inside it. Eventually, 8 double-pulley systems are designed; 4 to control MCP joints and 4 to control the correlated PIP and DIP joints. Figure 3.4 shows the design of a single double-pulley system.

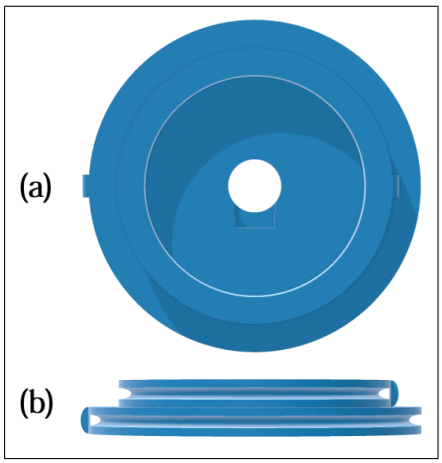

Figure 3.4 Double-pulley system design. (a) Front view. (b) Side view.

3.4.5 Hand Assembly

After 3D printing all the hand parts and pulleys, phalanges are attached together using stainless-steel pins through joints. Elastic tendons are passed through their tunnels and attached to their respective insertion point, then superglued to them to insure stability. For each finger, DIP is maximally flexed and its elastic flexor is attached unstarched. The same is applied for PIP extensor, where the joint is maximally extended and the elastic tendon is also attached unstarched. Following that, non-elastic tendons are superglued at their insertion points and passed through their tunnels.

To control pulleys rotation, servomotors are the actuators of choice. They were chosen due to their easy controllability compared to DC or BLDC motors. The specific model used is SG90 due to its availability and low cost. This micro servo is relatively small and light having a weight of 8 grams. It has a stall torque of 1.8 kg.cm and operates at 4.8 volts with a maximum power supply of 6 volts. They can rotate 180 degrees which is more than the desired maximum rotation of each pulley that equals to 114.6 degrees. The angle of the motor shaft is controlled using pule width modulation (Figure 3.5) [27]. Eight of these servos are used to control the 4 fingers, while the thumb is left without motors or tendons attached but still allowed to move its joints manually as it is outside the scope of this thesis.

Figure 3.5 SG90 servomotor [27].

The motors are fixed on four 3D printed columns to mimic the human arm. An elliptic base is designed, and 3D printed to hold the columns in place. The hand is fixed vertically and superglued to the columns for further stability. Motors controlling the index and middle fingers are set at 180 degree position while motors controlling the ring and little fingers are set at 0 degree position as the two sets of motors are positioned oppositely, and then the pulleys are fixed to the motors shafts. For each finger, the smaller pulley that controls MCP joint is positioned above the larger one controlling the interphalangeal joints in order to prevent interference between tendons and pulleys that are mechanically independent. The hand is set in such a way that all its fingers are maximally extended, and non-elastic tendons are pulled tightly, attached, and superglued to their pulleys. Figure 3.6 shows the hand after assembling all its part.

3.5 Fingers Control

Servomotors that transmit the force to fingers are controlled using Arduino microcontroller. The board of choice is Arduino MEGA 2560, since it has 12 PWM output pins which are enough to control the used 8 servos. The microcontroller is operated at 6-20 volts, which means that the external power supply used for the servos can also supply the Arduino board with power (Figure 3.7) [28].

To control the PWM output of the microcontroller, a code is written in a dedicated IDE in C++ programming language, and then uploaded to the Arduino board

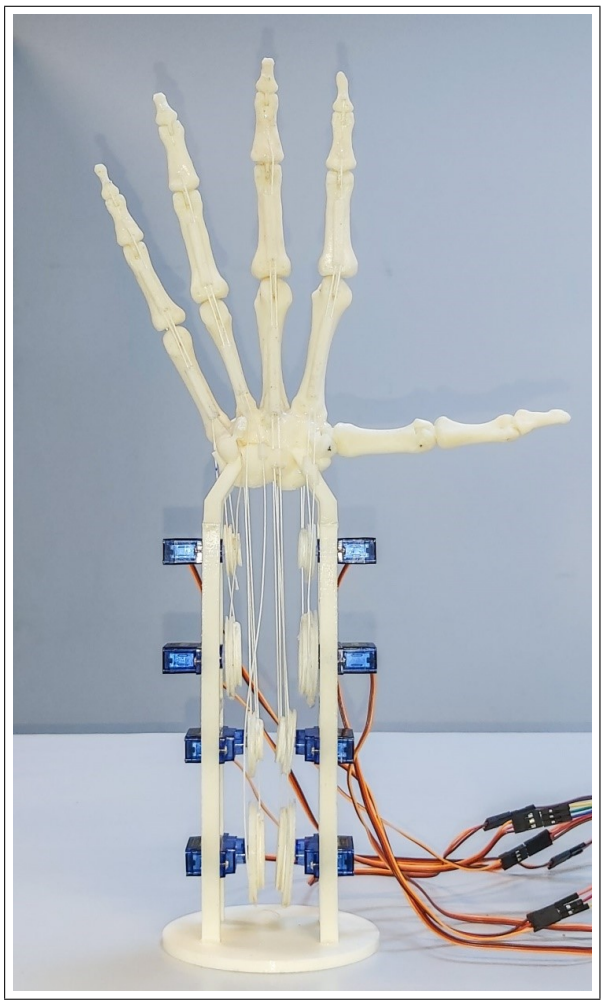

Figure 3.6 The anthropomorphic hand after assembly.

using USB cable. The power supply, servos and microcontroller are all grounded together to prevent voltage fluctuations, and the servos inputs are connected to Arduino PWM pins 5 to 12. Figure 3.8 shows a block diagram of the electrical components connections designed using Fritzing software.

Multiple codes are written to demonstrate different gestures. C++ instructions that are meant to flex or extend MCP joints and keep the interphalangeal joints unmoved take into account their dependency on each other that was found in the transfer functions, and coordination between both motors of each finger is necessary for this specific type of motion to eliminate that dependency which is not present in real life. To demonstrate the ability of the hand to produce different gestures, the microcontroller is programmed to perform 4 of them, which are:

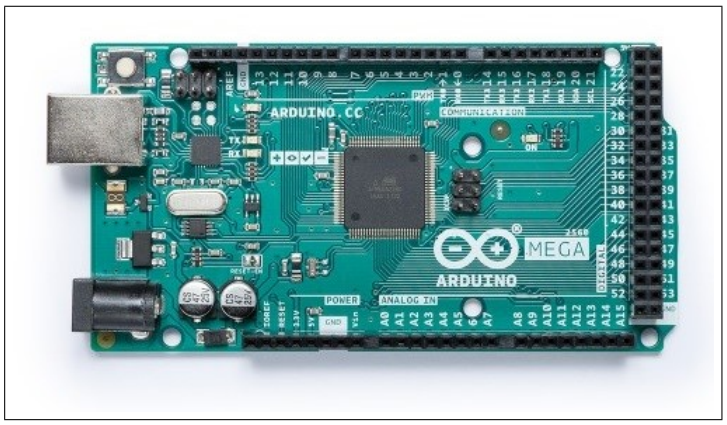

Figure 3.7 Arduino MEGA 2560 microcontroller [28].

- Full extension and flexion of all fingers together.
- Full extension and flexion of each finger independently.
- Full extension and flexion of the interphalangeal joints only.
- Full extension and flexion of the MCP joints only.

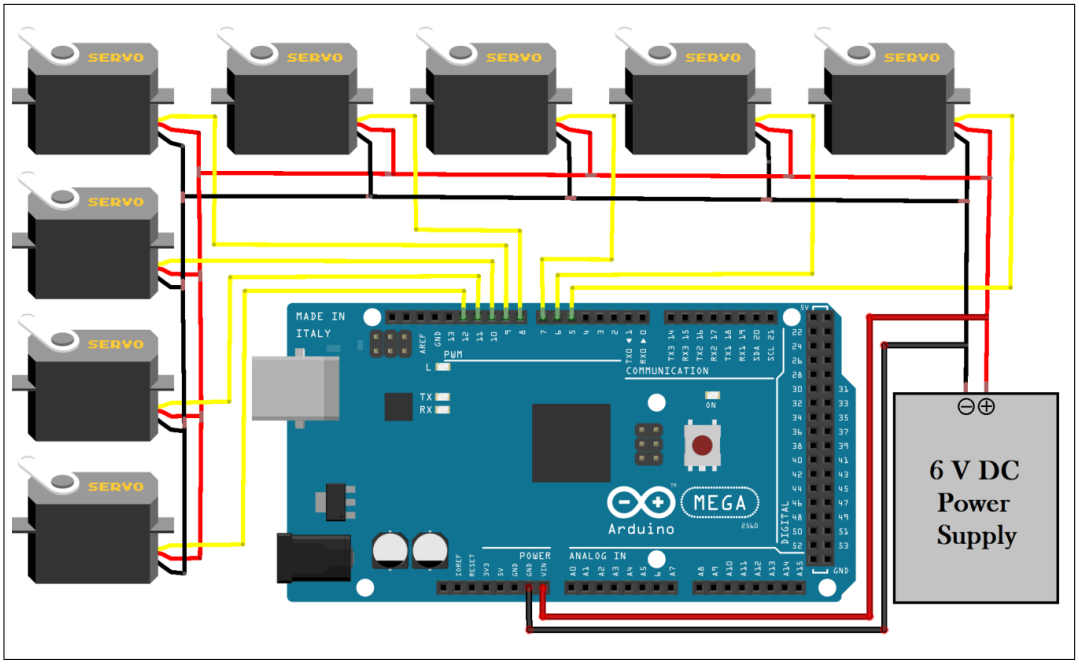

Figure 3.8 Block diagram of the electrical components connections.

3.6 Measuring Joint Angles

To test whether PIP and DIP angles of the designed hand satisfy the correlation found in human hands, those angles are measured using a transparent protractor at different flexion angles. For each finger, the motor controlling MCP joint is set at 5 evenly separated positions over its full range of motion. The fixed angles between the positions are based on the motor rotation; therefore, the angles are measured and reported. For each one of those 5 positions, the same process is followed for the motor controlling interphalangeal joints keeping in mind that MCP joint angle is fixed, covering the whole range of motion too. However, 10 data points are taken instead of 5 to get more accurate results. Consequently, 400 angles are measured and reported; of which half are PIP angles and the other half are DIP angles, and 20 correlation tests are to be conducted; 5 for each of the 4 finger with 10 data points per test.

SPSS software is used to perform 20 linear correlation tests, each producing a coefficient called Pearson's r; a measure that quantifies strength of the relationship between PIP and DIP angles.

4. RESULTS

In this study, kinematic models are built for the 4 fingers of an anthropomorphic hand with correlated PIP and DIP angles, of which the solutions are presented in this chapter in two parts; inverse kinematics for the finger angles in terms of fingertip position, and forward kinematics for tendon lengths change in terms of finger angles. The intended 4 hand gestures are shown and the results of PIP and DIP correlation tests are reported too.

4.1 Inverse Kinematics

For a typical 3-joint planar robot arm, there are infinite solutions to the inverse kinematics given the dependency of the 3 angles. However, two angles of each finger of the anthropomorphic hand are linearly correlated. This presents the possibility or having unique or finite solutions, but adds extra complexity to the workflow which is done based on Figure 4.1. The rotation matrix and its inverse in a 2D plane are:

$$R_\alpha = \begin{bmatrix} \cos\alpha & \sin\alpha \\ -\sin\alpha & \cos\alpha \end{bmatrix} \tag{4.1}$$

$$R_\alpha^{-1} = \begin{bmatrix} \cos\alpha & -\sin\alpha \\ \sin\alpha & \cos\alpha \end{bmatrix} \tag{4.2}$$

The position of the fingertip is calculated in terms of finger angles as:

$$(x, y) = R_\varphi(P + \ R_{\theta_1}(M + R_{\theta_2}D)) \tag{4.3}$$

Therefore, inverse kinematics can be solved as follows:

$$R_{\varphi}^{-1}(x, y) = P + \ R_{\theta_1}(M + R_{\theta_2} D) \tag{4.4}$$

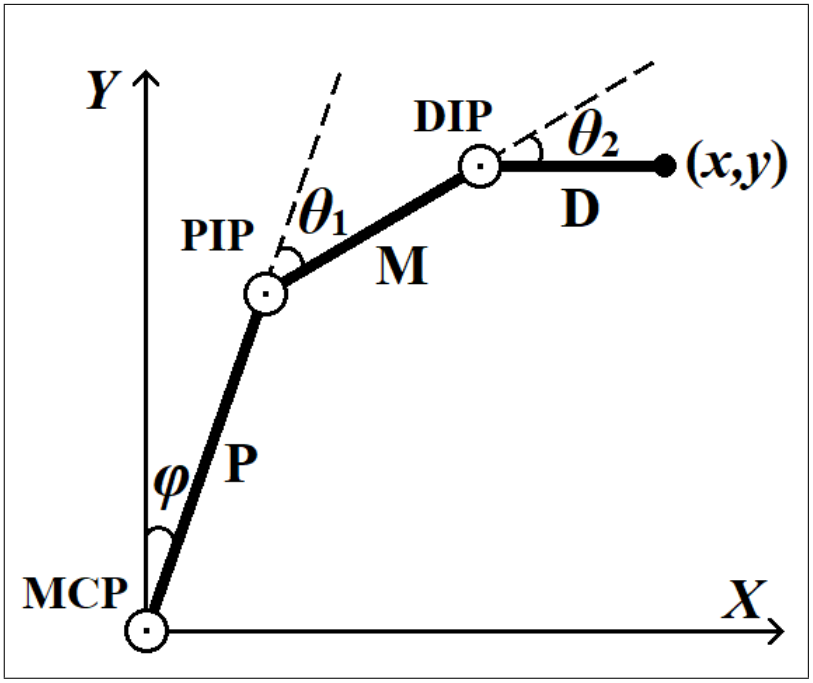

Figure 4.1 Model used for inverse kinematics.

Substituting, expanding and simplifying the matrices produces 2 equations:

$$x\cos\varphi - y\sin\varphi = M\sin\theta_1 + D\sin(\theta_1 + \theta_2) \tag{4.5}$$

$$x\sin\varphi + y\cos\varphi = P + M\cos\theta_1 + D\cos(\theta_1 + \theta_2) \tag{4.6}$$

Due to the correlation between DIP and PIP joints, a coefficient c that can be introduced to represent this linear relationship and to use a single angle for both joints such that:

$$\theta = \ \theta_1 = c\ \theta_2 \tag{4.7}$$

Substituting Eq. 4.7 in Eq. 4.5 and Eq. 4.6 gives:

$$x\cos\varphi - y\sin\varphi = M\sin\theta + D\sin(\theta + \frac{\theta}{c}) \tag{4.8}$$

$$x\sin\varphi + y\cos\varphi = P + M\cos\theta + D\cos(\theta + \frac{\theta}{c}) \tag{4.9}$$

The coefficient c depends on the range of motion for PIP and DIP joints, which are 0° to 105° and 0° to 85° respectively, meaning that c should equal to $\frac{105}{85}$ or 1.24. Substituting this value in Eq. 4.8 and Eq. 4.9 gives 2 equations that cannot be solved algebraically due to the resulting terms $\sin(\frac{190}{85}\theta)$ and $\cos(\frac{190}{85}\theta)$. This problem can be solved by assuming a more simple value for c that can produce an algebraic solution and still be acceptable for the model. The value $c = 1$ is close to the original value of 1.24 and it simplifies the equations to:

$$x\cos\varphi - y\sin\varphi = M\sin\theta + D\sin(2\theta) \tag{4.10}$$

$$x\sin\varphi + y\cos\varphi = P + M\cos\theta + D\cos(2\theta) \tag{4.11}$$

Squaring both equations, adding them, expanding and simplifying the result gives the following equation with the usage of trigonometric identities:

$$4PD\cos^2\theta + 2M\left(P + D\right)\cos\theta + P^2 + M^2 + D^2 - 2PD - x^2 - y^2 = 0 \tag{4.12}$$

This is a quadratic equation to which to the solution is:

$$\theta = \cos^{-1}\frac{-b \pm \sqrt{b^2 - 4ac}}{2a} \tag{4.13}$$

where:

$$a = 4PD \tag{4.14}$$

$$b = \ 2M\,(P + D) \tag{4.15}$$

$$c = \ P^2 + M^2 + D^2 - 2PD - x^2 - y^2 \tag{4.16}$$

The solution with the negative sign produces complex values or out of the range of motion for the angle θ, therefore, it is ignored and only the solution with the positive sign is considered.

Simulation of the model using Processing software is shown in Figure 4.2, where the angles are updated to place the fingertip at the position of mouse cursor. The range of motion of the fingertip is also calculated and plotted based on the joints' ranges of motion assumed to be from 0 to 100 degrees each. The updated values of the joints angles are also shown in real time.

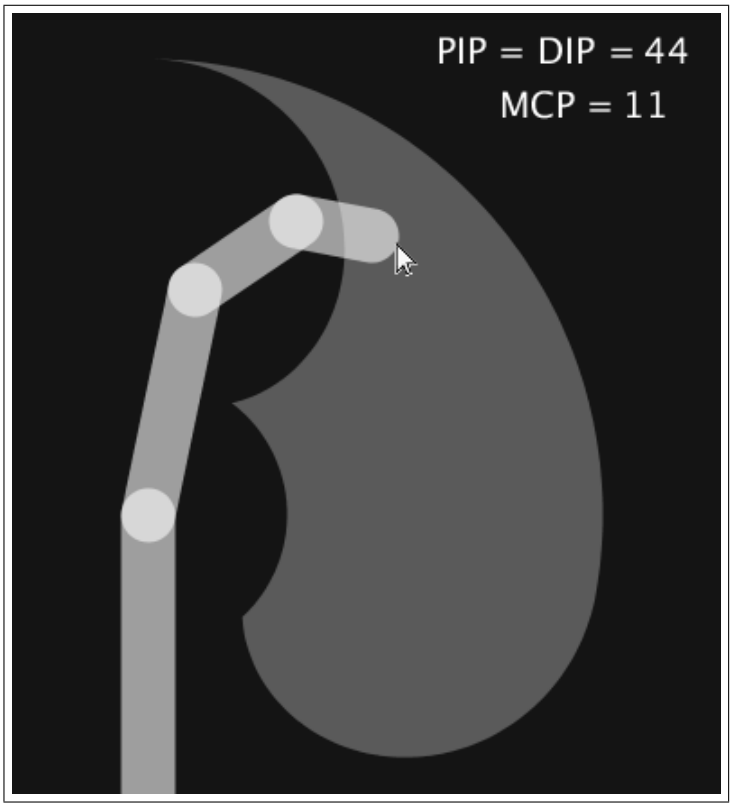

Figure 4.2 Simulation of the inverse kinematics.

4.2 Transfer Functions

To derive the relationship between the motors rotation and finger angles, the single finger model described in Chapter 2 is used. As mentioned before, an angle made by the end of a retinacular ligament at flexion side, the axis of joint rotation, and the beginning of the retinacular ligament of the adjacent phalanx at the same side is assumed to be the equal for both MCP and PIP joints at maximum extension equaling 120 degrees, and those 3 points form an isosceles triangle with the axis of rotation being its vertex and its legs labeled x on Figure 4.3. That specific angle was chosen be slightly larger than the maximum range of motion to avoid exceeding that range. DIP and PIP joints angles are assumed to be equal based on the results of the inverse kinematic model. Motor rotation causes change of non-elastic tendons length; therefore, transfer functions are represented as changes in tendons lengths. When the finger is flexed or extended, the lengths a_1, a_2, a_3, l_1, and l_2 change accordingly:

$$a_1 = \frac{\pi r \varphi}{180^\circ} \tag{4.17}$$

$$a_2 = \frac{\pi r \theta}{180^\circ} \tag{4.18}$$

$$a_3 = \frac{\pi r \theta}{180^\circ} \tag{4.19}$$

$$l_1 = \sqrt{2x^2 - 2x^2 \cos(120^\circ - \varphi)} = \sqrt{2}x\sqrt{1 - \cos(120^\circ - \varphi)} \tag{4.20}$$

$$l_2 = \sqrt{2x^2 - 2x^2 \cos(120^\circ - \theta)} = \sqrt{2}x\sqrt{1 - \cos(120^\circ - \theta)} \tag{4.21}$$

The length x can be calculated in terms of r as follows:

$$x = \frac{r}{\sin(30^\circ)} = 2r \tag{4.22}$$

The lengths l_1 and l_2 can be rewritten as:

$$l_1 = 2\sqrt{2}\ r\ \sqrt{1 - cos(120° - \varphi)} \tag{4.23}$$

$$l_2 = 2\sqrt{2}\ r\ \sqrt{1 - cos(120° - \theta)} \tag{4.24}$$

The initial length of l_1 and l_2 at full extension can be found by substituting 0 degrees in their equations, giving the same formula for both lengths:

$$l = 2\sqrt{2}\ r\ \sqrt{1 - cos(120° - 0)} = 2\sqrt{3}r \tag{4.25}$$

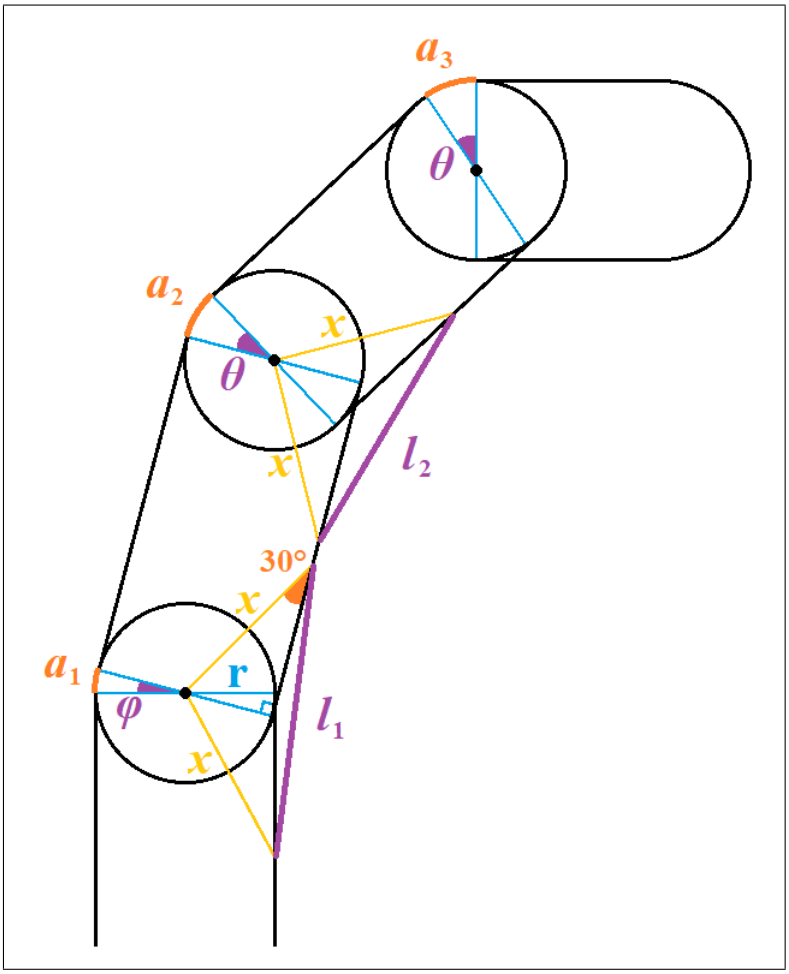

Figure 4.3 Model used to derive the transfer functions.

The changes in tendons length can be formulated as follows:

$$\Delta flexor_{MCP} = l - l_1 \tag{4.26}$$

$$\Delta extensor_{MCP} = a_1 \tag{4.27}$$

$$\Delta flexor_{PIP} = 2l - l_1 - l_2 \tag{4.28}$$

$$\Delta extensor_{DIP} = a_1 + a_2 + a_3 \tag{4.29}$$

By substituting the values of a_1, a_2, a_3, l_1, and l_2, transfer functions can be found:

$$\Delta flexor_{MCP}(\varphi) = r(2\sqrt{3} - 2\sqrt{2}\sqrt{1 - \cos(120^\circ - \varphi)}) \tag{4.30}$$

$$\Delta extensor_{MCP}(\varphi) = \frac{\pi r \varphi}{180^\circ} \tag{4.31}$$

$$\Delta flexor_{PIP}(\varphi, \theta) = r(4\sqrt{3} - 2\sqrt{2}(\sqrt{1 - \cos(120^\circ - \varphi)} + \sqrt{1 - \cos(120^\circ - \theta)})) \tag{4.32}$$

$$\Delta extensor_{DIP}(\varphi, \theta) = \frac{\pi r(\varphi + 2\theta)}{180^\circ} \tag{4.33}$$

The resulted functions show that changes in the lengths of tendons controlling MCP joint are only affected by the joint angle itself. Figure 4.4 is a plot of length change of MCP flexor tendon against MCP extensor tendon over the joint's full range of motion which is from 0 to 100 degrees. However, PIP flexor tendon and DIP extensor tendon change their lengths as a function of the interphalangeal joints as well as MCP joint, which implies a partial dependency between the three joints. Figure 4.5 shows multiple plots, each corresponds to a different value of MCP angle covering its full

range of motion and represents the length change of PIP flexor against DIP extensor over the two joints' full range of motion taken here to be from 0 to 100 degrees based on the previous inverse kinematic model. The length r in the model does not change during motion and does not have an effect on the ratio between the length change of each pair of tendons as it is algebraically omitted. Therefore, it is not considered as a variable affecting the lengths change and is assumed to equal 5 for the plots.

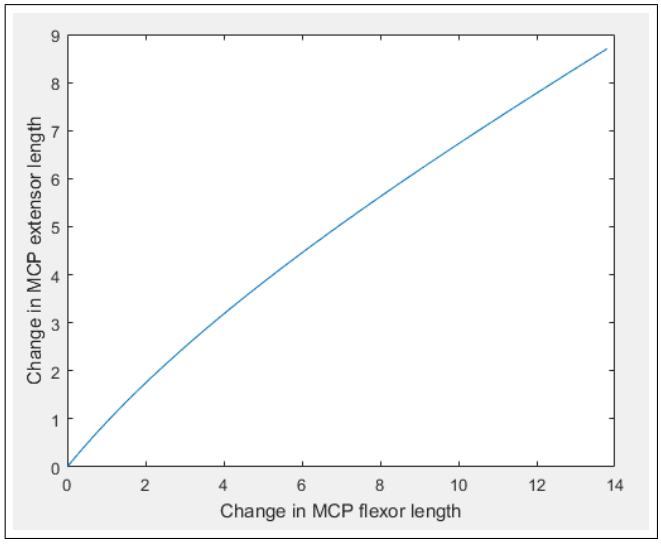

Figure 4.4 Change in MCP tendons lengths over their full range of motion.

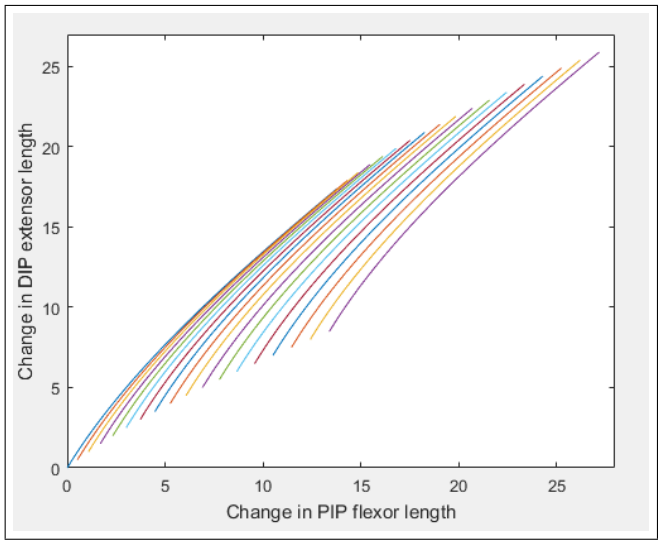

Figure 4.5 Change in interphalangeal tendons lengths over their full range of motion for different values of MCP joint angle.

4.3 Hand Gestures

The anthropomorphic hand was successfully able to perform the intended 4 gestures that can produce other variations too. Figure 4.6 shows those gestures at full flexion.

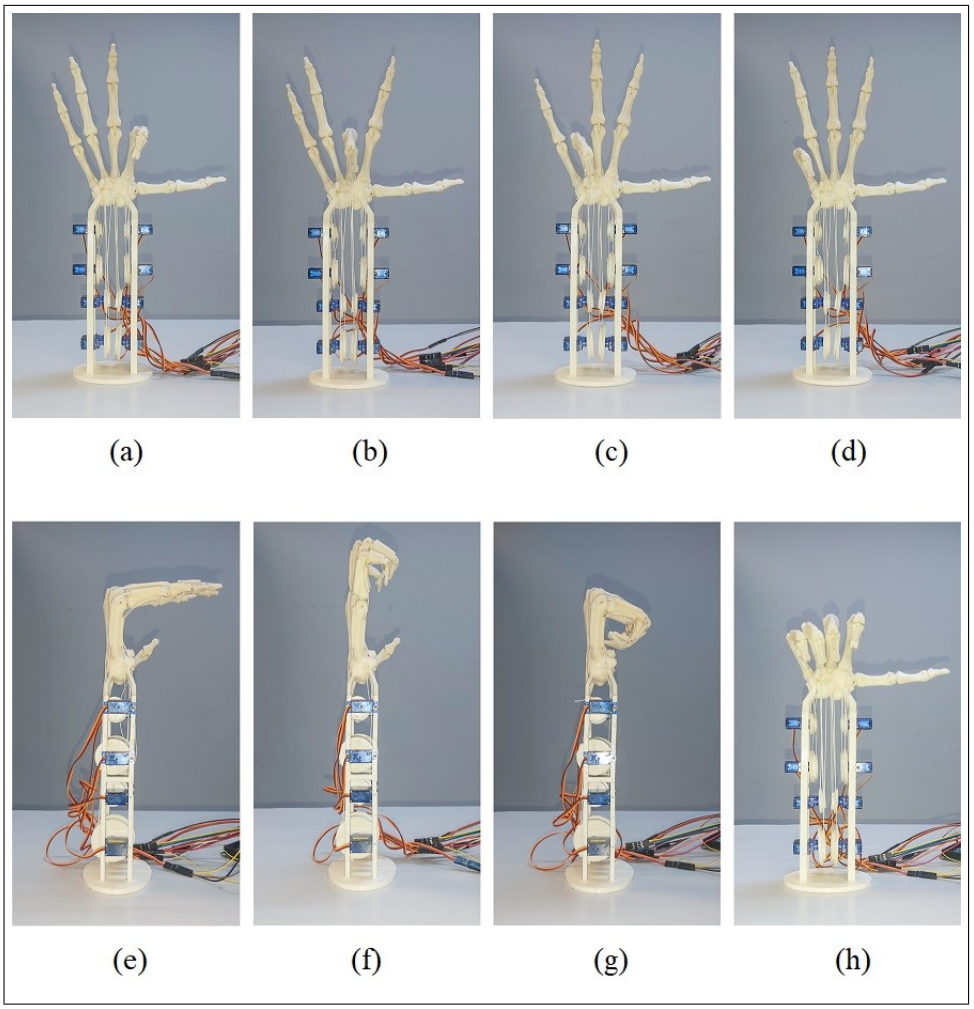

Figure 4.6 Hand gestures performed by the anthropomorphic hand. (a) Full flexion of index finger. (b) Full flexion of middle finger. (c) Full flexion of ring finger. (d) Full flexion of little finger. (e) Full flexion of all MCP joints.(f) Full flexion of all interphalangeal joints.(g & h) Full flexion of all joints.

4.4 Correlation between PIP and DIP angles

Correlations between interphalangeal joints for the designed hand are shown in Table 4.1 along with their significance. Among 20 reported correlations, 3 correlations

are significant at the 0.01 level, while the rest are significant at the 0.001 level. Interphalangeal joints angles are plotted against each other for the index finger (Figure 4.7), middle finger (Figure 4.8), ring finger (Figure 4.9), and little finger (Figure 4.10),

Table 4.1
Correlations between the designed interphalangeal joints. *: p≤0.05. **: pp≤0.01. ***: pp≤0.001.

Index Finger		Middle Finger		Ring Finger		Little Finger	
MCP angle	Correlation (Pearson's r)	MCP angle	Correlation (Pearson's r)	MCP angle	Correlation (Pearson's r)	MCP angle	Correlation (Pearson's r)
0	0.834**	0	0.965***	0	0.896***	0	0.868**
22	0.929***	31	0.969***	29	0.949***	32	0.917***
44	0.898***	53	0.944***	51	0.944***	49	0.928***
77	0.864**	82	0.968***	84	0.939***	81	0.937***
112	0.931***	119	0.973***	118	0.945***	120	0.947***

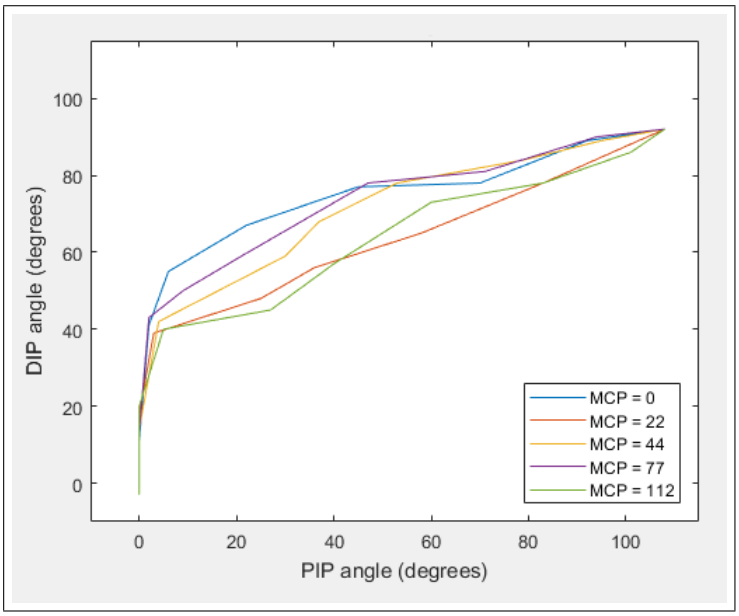

Figure 4.7 Measured index finger's angles during flexion.

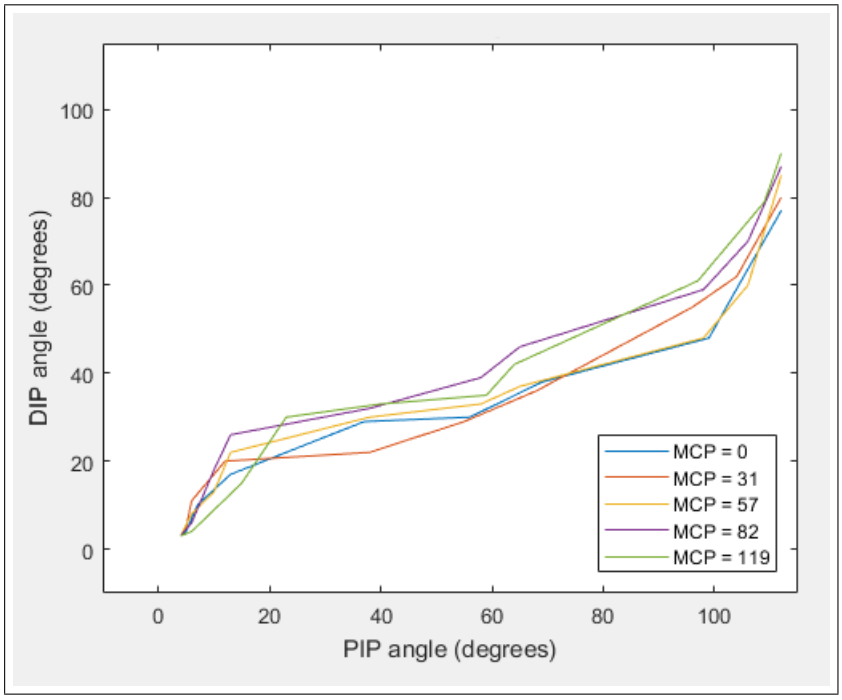

Figure 4.8 Measured middle finger's angles during flexion.

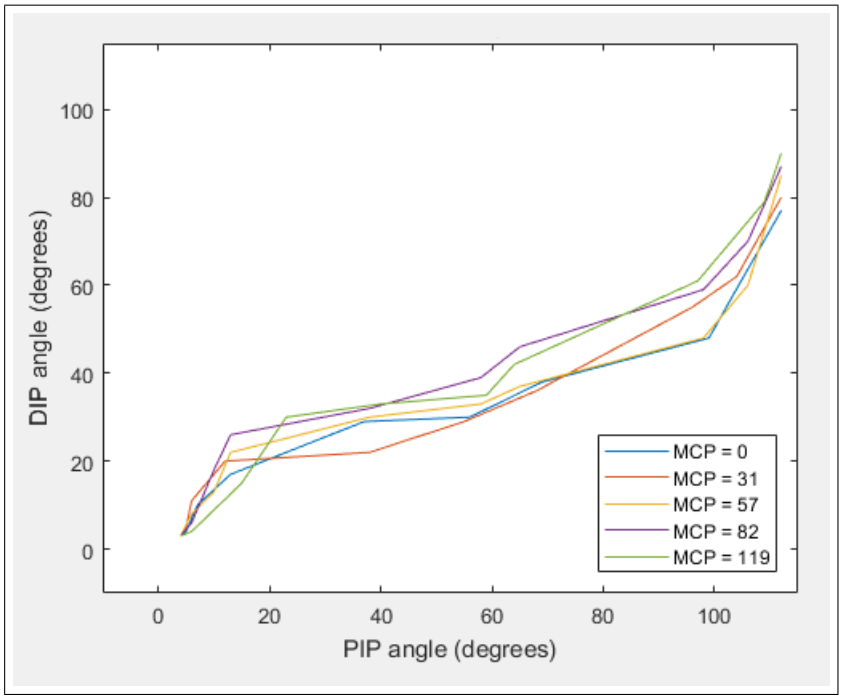

Figure 4.9 Measured ring finger's angles during flexion.

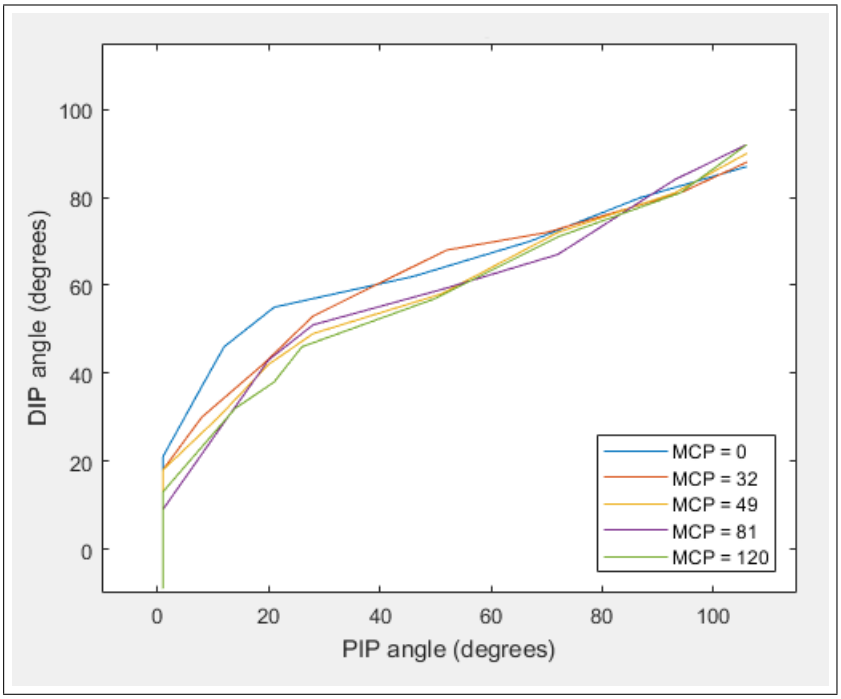

Figure 4.10 Measured little finger's angles during flexion.

5. DISCUSSION AND FUTURE WORK

5.1 Inverse Kinematics Model

The solution of the inverse kinematics shows that there exists a unique solution for the finger angles for each specific fingertip position in the 2D plane. This arises from the fact that even though there are 3 angles involved in the model, 2 of them are linearly correlated being PIP and DIP joint angles, which converts the model to a 2-angle problem, since one of the 3 original angles is just a linear function of another one. Therefore, this model can be thought as solving the inverse kinematics of a 2-joint arm with one main difference which is that the second arm changes its length as a function of the angle of correlation. Inverse kinematics for a 2-joint arm has 2 different solutions, but since the joint angles cannot be negative for our model only one solution is considered.

As has been shown in the results, an algebraic solution for the actual range of motion of the correlated joints cannot exist. However, approximation of the angles ratio from 1.24 down to 1 produces a solvable 2^{nd} order polynomial formula. Approximating the ratio up to 1.5 instead produces another solvable polynomial equation but of the 5^{th} order. Using a ratio that equals to 2 produces a 3^{rd} order polynomial equation. The first ratio was chosen since a 2^{nd} order polynomial equation is simpler and easier to solve and it is the closest to the original ratio.

Visualizing the solution shows that the fingertip has a range of motion of a special shape that is different than those of 2-joint and 3-joint arms. There are 2 reasons the range of motion is special; the limited range of angles motion and the PIP-DIP correlation.

5.2 Transfer Function and Pulleys Design

The main goal of deriving the transfer functions of the tendons is to realize the design of the pulleys. For each finger there are 2 pulley pairs, one pair controls 2 tendons that transmit a motor's force to MCP joint while the other pair controls the interphalangeal joints. The derived transfer functions describe the 2D geometric shape of the pulleys needed to generate the appropriate changes in tendons lengths. Taking the MCP-controlling pulley pair as an example, if the flexor pulley is designed to be a perfect circle then the other should be a spiral that changes its radius according to the ratio of length change between MCP flexor and extensor tendons. The same logic applies to the pulley pair that controls the interphalangeal joints.

The resulted transfer functions are nonlinear, and their plots show that each tendon pair has an increasing relationship. By looking at the graphs (Figures 4.4 and 4.5), the nonlinearity does not appear high, and the designed and 3D printed pulleys were all circles based on that observation, especially that there are no available tools to draw 3D spirals based on complex nonlinear functions. The requirement for the plots to be always increasing is to set the vertex' angle of the isosceles triangles xxl_1 and xxl_2 (Figure 4.3) to be larger than the range of motion of the joint that has the highest range, otherwise the physical implementation of the finger will cause the joints to fail reaching their maximum flexion possible.

Even though the relationship between the interphalangeal-controlling tendons depends on the supposedly uncorrelated MCP joint, all different plots shown in Figure 4.5 look to be identical but shifted in both x and y directions. This means that the motor rotation and the pulley design does not change for different MCP angles. However, initial extension and flexion lengths should be set for the interphalangeal-controlling tendons depending on the current MCP angle. This explains why the dependency of the interphalangeal pulleys on the MCP pulleys is only partial and does not imply correlation. In the physical implementation, this can be translated into coordination between the 2 motors of a single finger which can be reached by implementing the transfer functions in the software controlling the motors, not by

considering that dependency in the physical design which adds extra complexity to it. For that reason, 2 separate pulley pairs were designed for each finger, but the function controlling the interphalangeal pulleys in the Arduino code took into account the dependency on MCP angles which was assumed to be linear for the same reasons mentioned above.

5.3 Overall Design and Implementation

The hand showed an acceptable speed of fingers flexion and extension that was dependent on two factors; the maximum motor speed and the delays between angle-changing instructions in the Arduino code. The speed can be increased by using better motors which adds to the overall cost. When all motors work together at the same time, the power consumption was 2.53 Amperes at its maximum. Given that 6 volts are required to maximize the motors output, a separate battery can be used to allow portability. High temperature increase was noticed in the motors, which caused permanent damage in 3 of them and were replaced later. Using a relay that delivers power to the motors only when they move can solve that problem.

Friction was noticed between some of the 3D printed joints even though they were designed to have gaps that allow smooth motion. This was caused by slight imperfections in the prints adding some excess material; a problem that was solved by cleaning that excess material or repeating the print. The prints can be improved by using 3D printers with higher capabilities of printing with thinner layers and using better temperature regulations systems. Even though the material used for printing which is ULTRAT was chosen for its low fragility compared to other materials, one joint was broken due to repeated motion. This is because the dimensions of the joints are small, and they are limited by the dimensions of the phalanges. Solving this problem can be done by using metal joints instead of designing them as a part of the phalanges themselves.

Non-elastic tendons used in the design were all tightened during assembly. How-

ever, they showed loosening as the fingers flex and extend. This can be explained by the linear relationship on which the pulley design relies instead of the nonlinearity found by the mathematical model. Extra nonlinearity and hence tendons loosening is added due to the unique topology of every single phalanx, where each one does not have a consistent cross-section over its whole length, which complicates the mathematical modelling and generates different transfer functions for different fingers. One solution is to use cylindrical phalanges that have equal and consistent cross-sections, and to design pulleys with the nonlinear transfer functions. Another solution is to place the motors between joint so that they control them directly without the aid of pulleys and tendons. However, both solutions do not serve in the intended anthropomorphism since the bones shape in the first solution does not resemble those of humans, and the motor placement with the absence of tendons does not mimic the human hand's anatomy.

5.4 Correlation Analysis of the Designed Hand

As the results of PIP and DIP correlation show, all tests have shown correlations with Pearson's r coefficient higher than 0.8, which means that all correlations are strong [29]. Comparing that to the PIP-DIP correlation in human hand that equals to 0.986 [6], it can be said that the desired high correlation is present In the desired hand. This is also supported by the significance of all correlations.

The plots that represent PIP against DIP angles for the index, ring, and little fingers show a similar behavior. At the beginning of flexion, DIP angle increases rapidly while PIP angle remains constant or undergoes very small changes, then both angles start flexing together until PIP joint reaches its maximum flexion angle. This behavior can be a result of two factors. First, it can be caused by different forces and torques along the finger and its joints, such as friction between joints. Kinetic modelling of the finger can give more details about the contribution of different forces in causing this behavior. However, friction can be just a result of imperfections in the prints as mentioned before. The second factor is the usage of circular pulleys to represent linear transfer functions which are found by the model to be nonlinear. This was discussed

earlier this chapter as an explanation of loose tendons, which is noticed to be related to this behavior. The PIP flexor is loose at maximum extension of the finger. When flexion starts, it starts to tighten while DIP angle increases until the tendon is tight enough to flex the PIP joint. This kind of behavior is not highly noticed for the middle finger which might be due to its topology that evens out the nonlinearity.

For all fingers except for the index, the maximum DIP flexion angle increases as MCP angle increases. This is due to the dependency of PIP-DIP relationship on MCP joint angle that was discussed before. The DIP joint of the index finger always reaches its maximum flexion angle regardless the MCP joint angle. This may be a result of overstretching the elastic DIP flexor tendon during hand assembly.

5.5 Future Work

The main goal of this thesis is to model the PIP-DIP correlation to derive transfer functions that help in designing pulleys that control tendons. Since the nonlinear solution of the model was implemented here as linear for simplification, the next step is to find a solid way of designing pulleys with nonlinear relationships.

The model set for this thesis is merely kinematic, meaning that forces and torques are ignored. As was discussed before, forces might have an effect on the transfer functions that determine pulleys design especially at joint locations. By studying the hand kinetics in the future, such effects can be added to improve the transfer functions. This can also help deciding the appropriate motors to use in order to avoid overheating and damage caused to them, and provide better output and more consistent motion.

Since control is done using servomotors with no sensors, the only control variable available is the angle of motor shaft, which provides inaccurate information about the finger's state. To collect more reliable data about the hand's state, sensors can be added to provide information about the phalanges' orientation and applied forces on them to be used as feedback that serves in a more convenient way of control.

Only flexion and extension of the 4 fingers are considered for this thesis, but this is only a small step towards anthropomorphism. The next step would be studying the thumb in a similar manner to investigate if it is possible to decrease the number of used motors as was done here without affecting its motion. Adding the ability to adduct and abduct the 4 fingers also contributes to the intended anthropomorphism.

Anthropomorphic features considered in this thesis are the relationships between the finger's joins, hand bones anatomy, and the force transmissions method by using tendons and locating the motors in the arm. More anthropomorphic properties can be included in future studies such as studying the tensile properties of the used tendons, joints design, and retinacular ligaments design.

APPENDIX A. INSTRUCTIONS MANUAL FOR BUILDING THE HAND

This section is a step-by-step guide to build the hand that is introduced in this thesis. All required materials and components (other than the 3D printer and filaments) are listed in Table A.1. Additionally, 3D printing files for the hand parts are listed in Table A.2.

Table A.1
Parts and tools used in the anthropomorphic hand

Part	Count	Notes
SG90 micro servomotor	8	3 screws and different types of horns must be included with each motor
1 mm non-elastic synthetic thread	1	At least 10 meters long
1 mm stainless-steel bar	1	At least 25 cm long
Arduino MEGA board	1	-
Breadboard	1	-
DC power supply	1	-
Male-male jumper cable	27	-
Diagonal pliers	1	-
Cross slot screwdriver	1	-
Superglue	1	Recommended to be accompanied with activator

1- Parts numbered 1 to 15, which represent the phalanges, are 3D-printed with a layer thickness not more than 0.14 mm. Layer thicknesses that exceed this value were found to produce prints that have different dimensions than the desired ones. Filament material is recommended to be ABS, PETG, ULTRAT, or similar. PLA is not recommended due to its high rigidity that results in breaking the joints with

Table A.2
3D printing files

Part No.	File name	Description
1	1C.stl	Thumb's metacarpal bone
2	1P.stl	Thumb's proximal phalanx
3	1D.stl	Thumb's distal phalanx
4	2P.stl	Index finger's proximal phalanx
5	2M.stl	Index finger's middle phalanx
6	2D.stl	Index finger's distal phalanx
7	3P.stl	Middle finger's proximal phalanx
8	3M.stl	Middle finger's middle phalanx
9	3D.stl	Middle finger's distal phalanx
10	4P.stl	Ring finger's proximal phalanx
11	4M.stl	Ring finger's middle phalanx
12	4D.stl	Ring finger's distal phalanx
13	5P.stl	Little finger's proximal phalanx
14	5M.stl	Little finger's middle phalanx
15	5D.stl	Little finger's distal phalanx
16	wristMCP.stl	Wrist and metacarpal bones
17	pillars.stl	Motor pillars
18	base.stl	Hand base
19	p21.stl	Index finger's MCP pulley
20	p22.stl	Index finger's interphalangeal pulley
21	p31.stl	Middle finger's MCP pulley
22	p32.stl	Middle finger's interphalangeal pulley
23	p41.stl	Ring finger's MCP pulley
24	p42.stl	Ring finger's interphalangeal pulley
25	p51.stl	Little finger's MCP pulley
26	p52.stl	Little finger's interphalangeal pulley

repetitive motion. For this thesis, ULTRAT was used for its low fragility and shrinkage rate during printing. For the best result, it's recommended to place the phalanges on the printing plate at their posterior side to avoid adding loads of support around the joints. It's strongly recommended not to add any support inside the channels inside which the elastic and non-elastic tendons are supposed to pass, since any tiny excess material can introduce an obstacle that block the insertion of tendons.

2- Parts numbered 16 to 26, which represent the wrist and metacarpal bones, the pillars of the arm, the base and the pulleys are 3D-printed with a layer thickness not more than 0.14 mm. Filament material is recommended to be PLA since these parts are relatively large. Note that part 17 must be printed twice.

3- Servo motors are fixed on the pillars as shown in figure 3.6 with screws using a screwdriver. Note that for each pillar, the lower 2 motors are fixed such that their screws are applied from the shaft side of the motors, while the upper 2 motors are fixed such that their screws are applied from the opposite side of the motors. Note also that the shafts of all motors of a single pillar are all aligned at the same side, which is the opposite side of the alignment of motor shafts on the other pillar.

4- Motors are connected to Arduino MEGA, and then connected to the DC power supply as shown in figure 3.8. The voltage of the power supply must be set to be 6 volts, while the current is recommended to be at least 2.5 amperes.

5- Arduino code shown in Appendix B.1 is uploaded to the Arduino MEGA to set the initial positions of the motor shafts that correspond to full extension of the fingers. Board type and port number should be set correctly before uploading the code, and the power supply must be turned on.

6- For each motor, the horn with the single blade is cut in half such that it can fit tightly inside its dedicated space in each one of the pulleys.

7- Pulleys are fixed on the motors by plugging their horns into the motor shafts

while the power supply is turned on and Arduino MEGA is connected to the computer. Note that each motor has its own distinct pulley as shown in figure A.1. Note also that all pulleys must be fixed such that their horn blades are pointing exactly to the right as shown in figure A.2. Pulleys are secured in place using their dedicated screws.

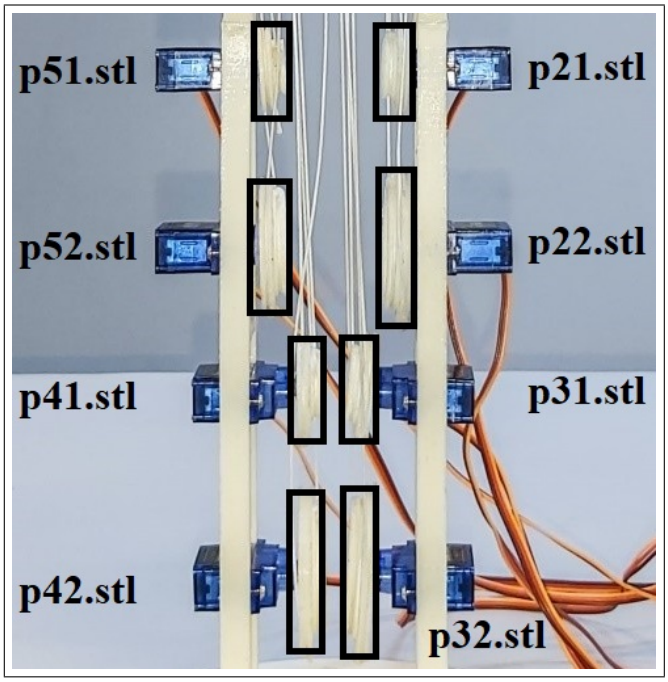

Figure A.1 Locations of pulley with respect to motors.

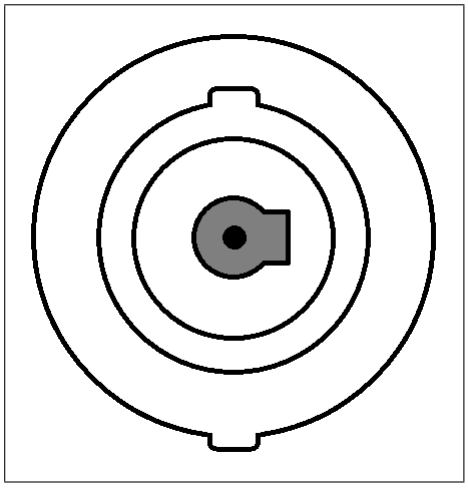

Figure A.2 Initial orientation of each pulley.

8- The power supply is turned off, and the pillars are attached to the base as shown in figure 3.6. To ensure stability, it's recommended to use superglue at the attachment site.

9- Parts numbered 1 to 16 are connected to each other to form the hand through joints. For each joint, the stainless-steel bar is cut to a length that can fit properly inside the joint, and then the two bones are joined together using the pin.

10- Elastic tendons are attached to the 4 fingers in a similar manner for each finger. For each tendon, a tight knot is made, superglued, and the other side of the tendon is passed inside its tunnel and pulled from the other side. While pulling, a second knot is made on the other side and superglued to the bone at the tunnel exit point, and the first knot is also superglued to the bone at the tunnel entrance point. The result should be such that the distal tendon is maximally flexing the DIP joint and the proximal tendon is maximally extending the PIP joint when no external force is applied to the joints (Figure A.3).

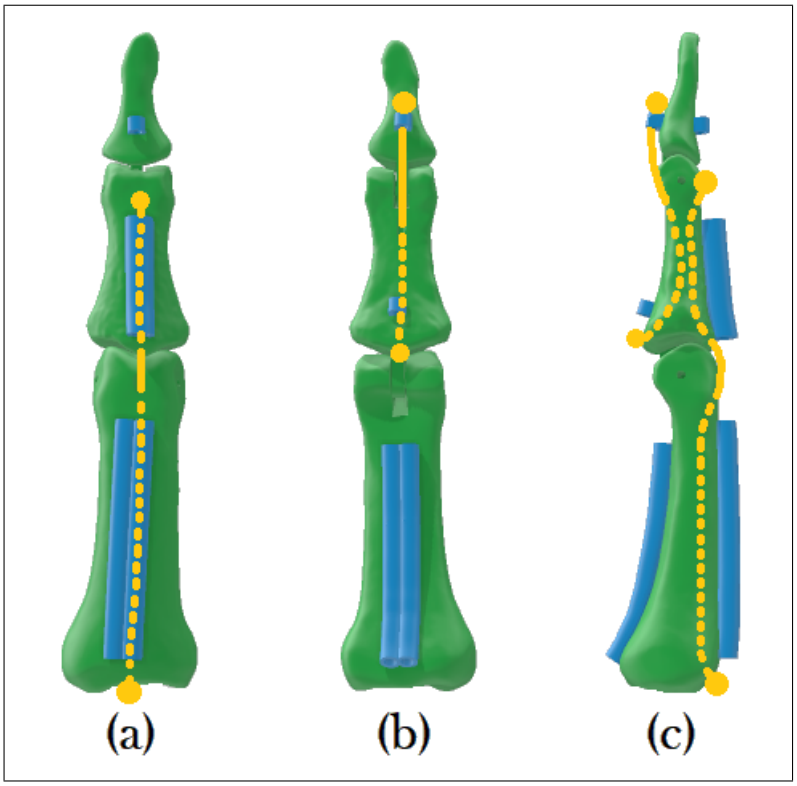

Figure A.3 Insertion of elastic tendons for one finger. (a) Back view. (b) Front view. (c) Side view.

11- Non-elastic tendons are attached to the 4 fingers in a similar manner for each finger. A total of 16 tendons are cut from the non-elastic thread, with a length of 60 cm each. For each tendon, a tight is made, superglued, and the other side of

the tendon is passed under the tendon's insertion point and then inside its tunnel or tunnels, and pulled from the other side. (Figure A.4).

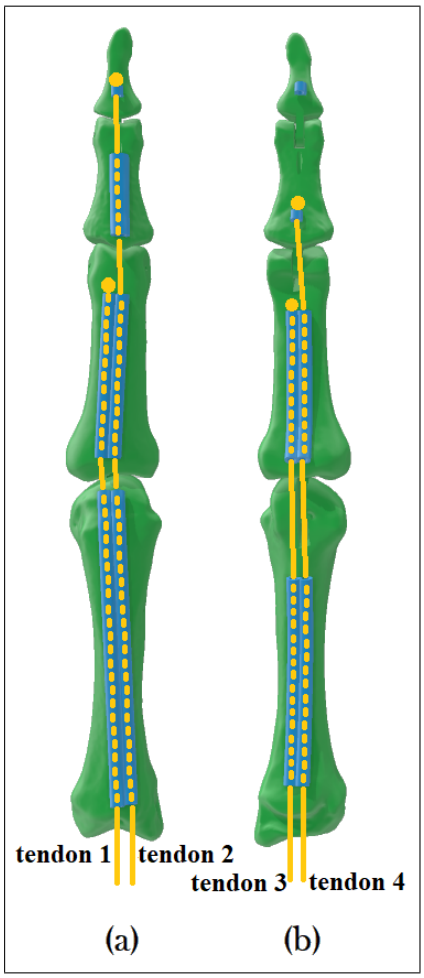

Figure A.4 Insertion of Non-elastic tendons for one finger. (a) Back view. (b) Front view.

12- Part 16 is attached to the top side of the pillars through the 4 attachment point using superglue as shown in figure 3.6.

13- The power source is turned on and the 4 non-elastic tendons of each finger are attached to their 2 pulleys as shown in figure A.5. When each tendon is attached to the pulley, it's pulled tightly and passed under its insertion point on the pulley, and then superglued to it while pulling. Each finger must be fully extended while its tendons are attached. It's recommended to start attaching the extension tendons first then the flexion tendons to ensure full extension.

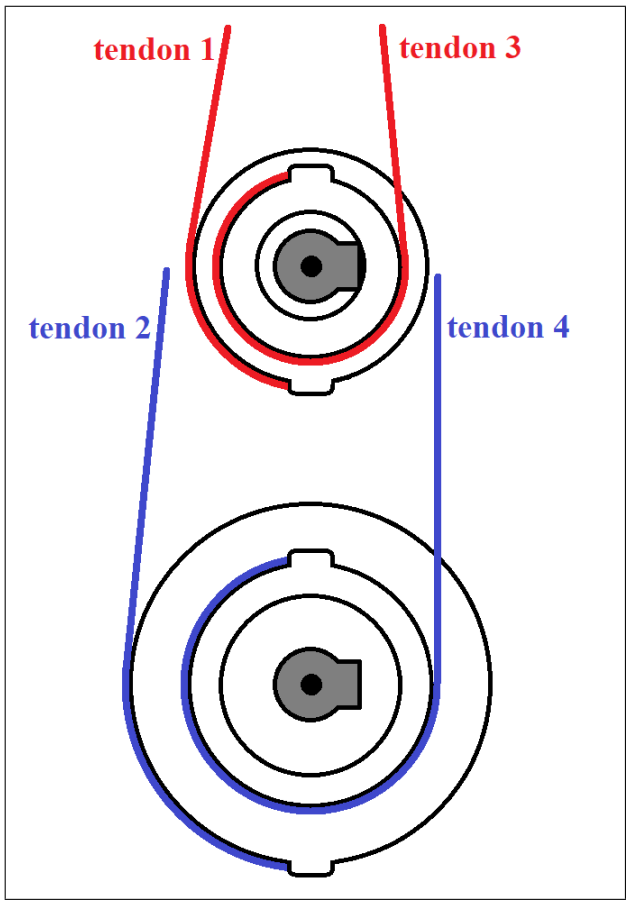

Figure A.5 Attaching tendons of one finger to their pulleys.

14- The Arduino program can be then changed by uploading different programs to produce various motions and gestsres (Appendix B).

APPENDIX B. ARDUINO CODES

B.1 Arduino Code for Initial Motor Positions

```
#include <Servo.h>

Servo IP2;

Servo MP2;

Servo IP3;

Servo MP3;

Servo IP4;

Servo MP4;

Servo IP5;

Servo MP5;

int f2[] = {11, 12, 180, 10, 160, 50};

int f3[] = {9, 10, 180, 10, 160, 50};

int f4[] = {7, 8, 10, 180, 50, 160};

int f5[] = {5, 6, 10, 180, 50, 160};
```

```
int Speed = 50; //the lower the faster

int longDelay = 1000;

int IP;

int MP;

void setup() {

IP2.attach(f2[0]);

MP2.attach(f2[1]);

IP3.attach(f3[0]);

MP3.attach(f3[1]);

IP4.attach(f4[0]);

MP4.attach(f4[1]);

IP5.attach(f5[0]);

MP5.attach(f5[1]);

IP2.write(f2[2]);

delay(1000);

MP2.write(f2[4]);
```

```
delay(1000);

IP3.write(f3[2]);

delay(1000);

MP3.write(f3[4]);

delay(1000);

IP4.write(f4[2]);

delay(1000);

MP4.write(f4[4]);

delay(1000);

IP5.write(f5[2]);

delay(1000);

MP5.write(f5[4]);

delay(1000); }
```

B.2 Arduino Code for Different Postures Demonstration

```
include <Servo.h>

Servo IP2;
```

```
Servo MP2;

Servo IP3;

Servo MP3;

Servo IP4;

Servo MP4;

Servo IP5;

Servo MP5;

int f2[] = {11, 12, 180, 10, 160, 50};

int f3[] = {9, 10, 180, 10, 160, 50};

int f4[] = {7, 8, 10, 180, 50, 160};

int f5[] = {5, 6, 10, 180, 50, 160};

int Speed = 50; //the lower the faster

int longDelay = 1000;

int IP;

int MP;

void setup() {
```

```
IP2.attach(f2[0]);

MP2.attach(f2[1]);

IP3.attach(f3[0]);

MP3.attach(f3[1]);

IP4.attach(f4[0]);

MP4.attach(f4[1]);

IP5.attach(f5[0]);

MP5.attach(f5[1]);

IP2.write(f2[2]);

delay(1000);

MP2.write(f2[4]);

delay(1000);

IP3.write(f3[2]);

delay(1000);

MP3.write(f3[4]);

delay(1000);
```

```
IP4.write(f4[2]);

delay(1000);

MP4.write(f4[4]);

delay(1000);

IP5.write(f5[2]);

delay(1000);

MP5.write(f5[4]);

delay(1000);

}

void loop() {

FullFlex2();

FullExtend2();

FullFlex3();

FullExtend3();

FullFlex4();

FullExtend4();
```

```
FullFlex5();

FullExtend5();

FullClose();

FullOpen();

MCPclose();

MCPopen();

IPclose();

IPopen(); }

void FullFlex2() {

for (int i = 1 ; i <= Speed ; i++) {

IP = map(i, 1, Speed, f2[2], f2[3]);

MP = map(i, 1, Speed, f2[4], f2[5]);

IP2.write(IP);

MP2.write(MP);

delay(15);

}
```

```
delay(longDelay);

}

void FullFlex3() {

for (int i = 1 ; i <= Speed ; i++) {

IP = map(i, 1, Speed, f3[2], f3[3]);

MP = map(i, 1, Speed, f3[4], f3[5]);

IP3.write(IP);

MP3.write(MP);

delay(15);

}

delay(longDelay);

}

void FullFlex4() {

for (int i = 1 ; i <= Speed ; i++) {

IP = map(i, 1, Speed, f4[2], f4[3]);

MP = map(i, 1, Speed, f4[4], f4[5]);
```

```
IP4.write(IP);

MP4.write(MP);

delay(15);

}

delay(longDelay);

}

void FullFlex5() {

for (int i = 1 ; i <= Speed ; i++) {

IP = map(i, 1, Speed, f5[2], f5[3]);

MP = map(i, 1, Speed, f5[4], f5[5]);

IP5.write(IP);

MP5.write(MP);

delay(15);

}

delay(longDelay);

}
```

```
void FullExtend2() {

for (int i = Speed ; i >= 1 ; i–) {

IP = map(i, 1, Speed, f2[2], f2[3]);

MP = map(i, 1, Speed, f2[4], f2[5]);

IP2.write(IP);

MP2.write(MP);

delay(15);

}

delay(longDelay);

}

void FullExtend3() {

for (int i = Speed ; i >= 1 ; i–) {

IP = map(i, 1, Speed, f3[2], f3[3]);

MP = map(i, 1, Speed, f3[4], f3[5]);

IP3.write(IP);

MP3.write(MP);
```

```
delay(15);

}

delay(longDelay);

}

void FullExtend4() {

for (int i = Speed ; i >= 1 ; i–) {

IP = map(i, 1, Speed, f4[2], f4[3]);

MP = map(i, 1, Speed, f4[4], f4[5]);

IP4.write(IP);

MP4.write(MP);

delay(15);

}

delay(longDelay);

}

void FullExtend5() {

for (int i = Speed ; i >= 1 ; i–) {
```

```
IP = map(i, 1, Speed, f5[2], f5[3]);

MP = map(i, 1, Speed, f5[4], f5[5]);

IP5.write(IP);

MP5.write(MP);

delay(15);

}

delay(longDelay);

}

void FullClose() {

for (int i = 1 ; i <= Speed ; i++) {

int IP2c = map(i, 1, Speed, f2[2], f2[3]);

int MP2c = map(i, 1, Speed, f2[4], f2[5]);

int IP3c = map(i, 1, Speed, f3[2], f3[3]);

int MP3c = map(i, 1, Speed, f3[4], f3[5]);

int IP4c = map(i, 1, Speed, f4[2], f4[3]);

int MP4c = map(i, 1, Speed, f4[4], f4[5]);
```

```
int IP5c = map(i, 1, Speed, f5[2], f5[3]);

int MP5c = map(i, 1, Speed, f5[4], f5[5]);

delay(15);

IP2.write(IP2c);

MP2.write(MP2c);

IP3.write(IP3c);

MP3.write(MP3c);

IP4.write(IP4c);

MP4.write(MP4c);

IP5.write(IP5c);

MP5.write(MP5c);

}

delay(longDelay);

}

void FullOpen() {

for (int i = Speed ; i >= 1 ; i–) {
```

```
int IP2c = map(i, 1, Speed, f2[2], f2[3]);

int MP2c = map(i, 1, Speed, f2[4], f2[5]);

int IP3c = map(i, 1, Speed, f3[2], f3[3]);

int MP3c = map(i, 1, Speed, f3[4], f3[5]);

int IP4c = map(i, 1, Speed, f4[2], f4[3]);

int MP4c = map(i, 1, Speed, f4[4], f4[5]);

int IP5c = map(i, 1, Speed, f5[2], f5[3]);

int MP5c = map(i, 1, Speed, f5[4], f5[5]);

IP2.write(IP2c);

MP2.write(MP2c);

IP3.write(IP3c);

MP3.write(MP3c);

IP4.write(IP4c);

MP4.write(MP4c);

IP5.write(IP5c);

MP5.write(MP5c);
```

```
delay(15);

}

delay(longDelay);

}

void MCPclose() {

for (int i = 1 ; i <= Speed ; i++) {

int IP2c = map(i, 1, Speed, f2[2], 120);

int MP2c = map(i, 1, Speed, f2[4], f2[5]);

int IP3c = map(i, 1, Speed, f3[2], 120);

int MP3c = map(i, 1, Speed, f3[4], f3[5]);

int IP4c = map(i, 1, Speed, f4[2], 70);

int MP4c = map(i, 1, Speed, f4[4], f4[5]);

int IP5c = map(i, 1, Speed, f5[2], 70);

int MP5c = map(i, 1, Speed, f5[4], f5[5]);

delay(15);

IP2.write(IP2c);
```

```
MP2.write(MP2c);

IP3.write(IP3c);

MP3.write(MP3c);

IP4.write(IP4c);

MP4.write(MP4c);

IP5.write(IP5c);

MP5.write(MP5c);

}

delay(longDelay);

}

void MCPopen() {

for (int i = Speed ; i >= 1 ; i–) {

int IP2c = map(i, 1, Speed, f2[2], 120);

int MP2c = map(i, 1, Speed, f2[4], f2[5]);

int IP3c = map(i, 1, Speed, f3[2], 120);

int MP3c = map(i, 1, Speed, f3[4], f3[5]);
```

```
int IP4c = map(i, 1, Speed, f4[2], 70);

int MP4c = map(i, 1, Speed, f4[4], f4[5]);

int IP5c = map(i, 1, Speed, f5[2], 70);

int MP5c = map(i, 1, Speed, f5[4], f5[5]);

IP2.write(IP2c);

MP2.write(MP2c);

IP3.write(IP3c);

MP3.write(MP3c);

IP4.write(IP4c);

MP4.write(MP4c);

IP5.write(IP5c);

MP5.write(MP5c);

delay(15);

}

delay(longDelay);

}
```

```
void IPclose() {

for (int i = 1 ; i <= Speed ; i++) {

int IP2c = map(i, 1, Speed, f2[2], 70);

int IP3c = map(i, 1, Speed, f3[2], 70);

int IP4c = map(i, 1, Speed, f4[2], 120);

int IP5c = map(i, 1, Speed, f5[2], 120);

delay(15);

IP2.write(IP2c);

IP3.write(IP3c);

IP4.write(IP4c);

IP5.write(IP5c);

}

delay(longDelay);

}

void IPopen() {

for (int i = Speed ; i >= 1 ; i–) {
```

```
int IP2c = map(i, 1, Speed, f2[2], 70);

int IP3c = map(i, 1, Speed, f3[2], 70);

int IP4c = map(i, 1, Speed, f4[2], 120);

int IP5c = map(i, 1, Speed, f5[2], 120);

IP2.write(IP2c);

IP3.write(IP3c);

IP4.write(IP4c);

IP5.write(IP5c);

delay(15);

}

delay(longDelay);

}
```

REFERENCES

1. Drake, R., A. Vogl, A. Mitchell, R. Tibbitts, and R. E. P. in *Grays Atlas of Anatomy, Elsevier - Health Sciences Div*, p. 426, 2014.

2. Themes, U., "The forearm, wrist, and hand," *Musculoskeletal Key*, 2016. [Online]. Available: https://musculoskeletalkey.com/the-forearm-wrist-and-hand-3.

3. Xu, Z., and E. Todorov, "Design of a highly biomimetic anthropomorphic robotic hand towards artificial limb regeneration," in *2016 IEEE International Conference on Robotics and Automation (ICRA)*, 2016.

4. Atasoy, A., E. Kaya, E. Toptas, S. Kuchimov, E. Kaplanoglu, and M. Ozkan, "24 dof emg controlled hybrid actuated prosthetic hand," in *38th Annual International Conference of the IEEE Engineering in Medicine and Biology Society (EMBC*, 2016.

5. Zwieten, K., K. Schmidt, G. Bex, P. Lippens, and W. Duyvendak, "An analytical expression for the d.i.p. - p.i.p. flexion interdependence in human fingers," *Acta of bioengineering and biomechanics / Wroclaw University of Technology*, Vol. 17, no. 1, pp. 129–135, 2015.

6. Hahn, P., H. Krimmer, A. Hradetzky, and U. Lanz, "Quantitative analysis of the linkage between the interphalangeal joints of the index finger," *Journal of Hand Surgery*, Vol. 20, no. 5, pp. 696–699, 1995.

7. ElKoura, K., and K. Singh, "Handrix: Animating the human hand," in *Proceedings of the 2003 ACM SIGGRAPH/Eurographics Symposium on Computer Animation*, pp. 110–119, 2003.

8. Jones, L., and J. S. Lederman, *Human hand function*, New York: Oxford University Press, 2007.

9. Schuenke, M., L. Ross, E. Lamperti, E. Schulte, and U. in *Atlas of Anatomy: General Anatomy and Musculoskeletal System*, pp. 222–225, Stuttgart, NY: Thieme, 2006.

10. Baksa, G., P. Mandl, S. Benis, L. Patonay, G. Balint, and P. Balint, "Gross anatomy of the human hand," in *Ultrasonography of the Hand in Rheumatology*, pp. 15–41, 2018.

11. Melo, E., O. Sánchez, and D. Hurtado, "Anthropomorphic robotic hands: a review," *Ingenierìa y Desarrollo*, Vol. 32, no. 2, pp. 279–313, 2014.

12. Yang, J., E. Pitarch, K. Abdel-Malek, A. Patrick, and L. Lindkvist, "A multi-fingered hand prosthesis," *Mechanism and Machine Theory*, Vol. 39, no. 6, pp. 555–581, 2004.

13. Birglen, L., T. Lalibertè, and C. Gosselin, "Grasping vs. manipulating," in *Springer Tracts in Advanced Robotics Underactuated Robotic Hands*, pp. 7–31, 2008.

14. Yong, K., Y. Ge, H. Cao, and L. He, "A multi-sensor system applied to control an intelligent robotic hand for underwater environment," in *2009 International Conference on Mechatronics and Automation*, 2009.

15. Diftler, M., F. Permenter, B. Hargrave, R. Platt, R. Savely, R. Ambrose, J. Mehling, M. Abdallah, N. Radford, L. Bridgwater, A. Sanders, R. Askew, D. Linn, and J. Yamokoski, "Robonaut 2 - the first humanoid robot in space," in *2011 IEEE International Conference on Robotics and Automation*, 2011.

16. Liu, H., K. Wu, P. Meusel, G. Hirzinger, M. Jin, Y. Liu, S. Fan, T. Lan, and Z. Chen, "A dexterous humanoid five-fingered robotic hand," in *RO-MAN 2008 - The 17th IEEE International Symposium on Robot and Human Interactive Communication*, 2008.

17. Slade, P., A. Akhtar, M. Nguyen, and T. Bretl, "Tact: Design and performance of an open-source, affordable, myoelectric prosthetic hand," in *2015 IEEE International Conference on Robotics and Automation (ICRA)*, 2015.

18. Wang, C., Y. Sun, J. Xu, X. Liu, X. Zhou, and X. Chen, "The design and development of an anthropomorphic worm-gear driven robotic hand: Bit-jocko," in *2019 IEEE 4th International Conference on Advanced Robotics and Mechatronics (ICARM*, 2019.

19. Tan, S., W. Zhang, Q. Chen, and D. Du, "Design and analysis of underactuated humanoid robotic hand based on slip block-cam mechanism," in *2009 IEEE International Conference on Robotics and Biomimetics (ROBIO*, 2009.

20. Roccella, S., M. Carrozza, G. Cappiello, M. Zecca, H. Miwa, K. Ltoh, M. Matsumoto, P. Dario, J. Cabibihan, and A. Takanishi, "Design, fabrication and preliminary results of a novel anthropomorphic hand for humanoid robotics: Rch-1," in *2004 IEEE/RSJ International Conference on Intelligent Robots and Systems (IROS*, 2004. IEEE Cat. No.04CH37566).

21. Gaiser, I., S. Schulz, A. Kargov, H. Klosek, A. Bierbaum, C. Pylatiuk, R. Oberle, T. Werner, T. Asfour, G. Bretthauer, and R. Dillmann, "A new anthropomorphic robotic hand," in *Humanoids 2008 - 8th IEEE-RAS International Conference on Humanoid Robots*, 2008.

22. Martell, J., and G. Gini, "Robotic hands: Design review and proposal of new design process," *International Journal of Applied Mathematics and Computer Sciences*, Vol. 4, no. 2, pp. 587–592, 2007.

23. Holguin, P., A. Rico, L. Gomez, and L. Munuera, "The coordinate movement of the interphalangeal joints," *Clinical Orthopaedics and Related Research*, Vol. 362, 1999.

24. Thingiversecom, "Human hand bones - thumb by siderits," [Online]. Available: https://www.thingiverse.com/thing:15342.

25. Rodríguez-Panes, A., J. Claver, and A. Camacho, "The influence of manufacturing parameters on the mechanical behaviour of PLA and ABS pieces manufactured by FDM: A comparative analysis," *Materials*, Vol. 11, no. 8, p. 1333, 2018.

26. Hume, M., H. Gellman, H. Mckellop, and R. Brumfield, "Functional range of motion of the joints of the hand," *The Journal of Hand Surgery*, Vol. 15, no. 2, pp. 240–243, 1990.

27. "SG90 servo. datasheet pdf. equivalent," [Online]. Available: https://datasheetspdf.com/pdf/791970/TowerPro/SG90/1.

28. "Arduinoboardmega2560," *Arduino*. [Online]. Available: https://www.arduino.cc/en/pmwiki.php?n=Main%2FarduinoBoardMega2560.

29. Akoglu, H., "User's guide to correlation coefficients," *Turkish Journal of Emergency Medicine*, Vol. 18, no. 3, pp. 91–93, 2018.